Contents

Chapter 1

Introduction

In astrophysics much attention is paid to the evolution of massive stars and to the compact objects they evolve into. Especially the very explosive events of supernovae and Gamma Ray Bursts are subject of both observational and theoretical research, because they are thought to be connected to the formation of black holes. These catastrophic events are the melting pots in the universe and produce much of the heavy metals that can not be produced in the stars itself. Since metals are of invaluaeble worth for the life on earth, it is worth to investigate the processes and sites in which these elements are formed. Problematic in this case, is the fact that once a black hole is formed, it is not possible to investigate it, since we can not get any information out of it. Black holes are isolated islands in the universe, however there are systems in which we can, indirectly, gather information about the black hole and the evolution of its progenitor. These systems are the black hole binaries, systems that contain a black hole and a non-compact companion.

The research decribed in this thesis is focussed on low mass black hole binaries (LMBHBs), that consist of a black hole and a low mass companion. These companions are, of low mass, and hence main sequence or late main sequence stars. Since main sequence evolution is rather simple, LMBHBs are an excellent possiblity to obtain information about the system itself and the foregoing evolution, especially when they are visible as X-ray sources. This is the case if the secondary fills its Roche lobe and transfers mass onto the black hole.
A very interesting system is the LMBHB GRO J1655-40. The primary is a black hole with a mass between 5.0 and 7.5 $M_\odot$, that possibly rotates at a maximum spinrate. The secondary is a Roche lobe filling star with a mass between 1.1 and 2.8 $M_\odot$. The evolutionary state of the secondary is still debated. The system is a transient X-ray source, which means that active phases in which the system is very bright in X-ray emission are alternated with quiescent phases in which the system completely vanishes in X-ray and the secondary only is detectable in the optical. Sensational were the detection of superluminal outflows in the form of two polar jets in august 1994.

The goal of this thesis is to make, on theoretical grounds, a decision of the mass of the secondary and its evolutionary state, as from the observers side it seems impossible to answer this question. In order to reach this goal, detailed evolutionary models were calculated, but as we will see in Chapter 3, they cannot give final answers and their worth is disputable, because of the trail-and-error nature of this approach. There, however, is one conclusion that can be drawn, also suggested by other authors; that the secondary is probably a Roche lobe filling main sequence star.
To avoid again a trail-and-error method, we developed a new method, based on the relation between the luminosity, mass and mean molecular weight of a star, that reconstructs, step-by-step, a stellar model which displays similar observable properties as the observed star. Within reasonable errors, we are able to calculate with this method, the actual mass of the star and also the original zero-age main sequence mass.
Details of this new method can be found in Chapter 4 and Chapter 5. The application to two observations of GRO J1655-40 by Orosz & Bailyn (1997) and Beer & Podsiadlowski (2002) can also be found in Chapter 5.
The overall discussion of this system is done Chapter 6, in which the results of the detailed binary evolutionary models of Chapter 3 and the numerical models of Chapter 5 are compared.

Arend Jan Poelarends

Utrecht, October 21 2002

Chapter 2

X-ray Binaries

The number of X-ray sources detected so far with several observatories is of the order of 150000 (Rosat website, 2002), rather higher than the number of stars visible with the naked eye. The majority of the brighter of these sources are located near the galactic plane (see Fig. 2.1) and are neutron stars or black holes that accrete matter from an accompanying star (Verbunt, 2001). In this

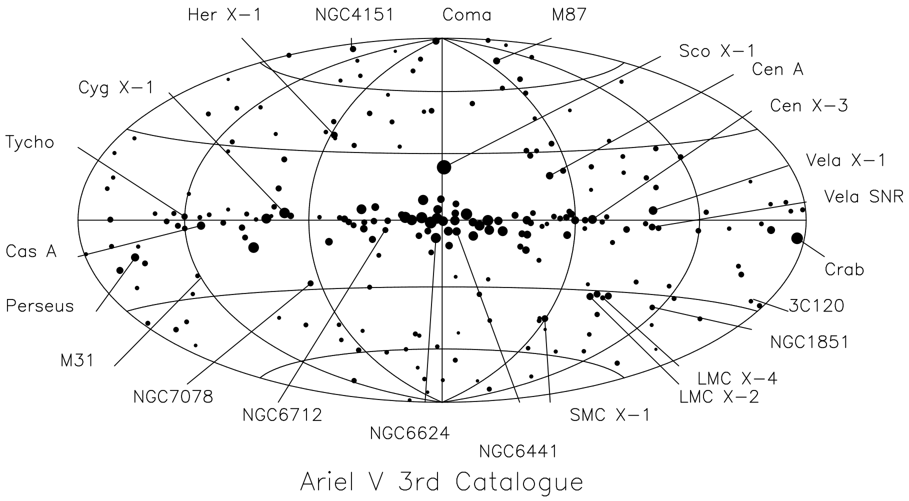

Figure 2.1: Map of X-ray point sources in Galactic Coordinates. The bright sources plotted in this figure are obtained by the Ariel V satellite. The size of the symbols is larger for more luminous sources. The sources are in part X-ray binaries (Her X-1, Cyg X-1, Sco X-1, Cen X-3, Vela X-1), supernova remnants (Crab, Vela, Cas A, Tycho), nearby Galaxies (M31, Magellanic Clouds), black holes in galaxies (Cen A, M87, NGC4151, 3C120), and clusters of galaxies (Coma, Perseus).(Verbunt, 2000, after McHardy et al. 1981)

chapter we describe some theoretical considerations in the framework of binary evolution, with emphasis on mass transfer to neutron stars and black holes.

2.1 The Roche Potential

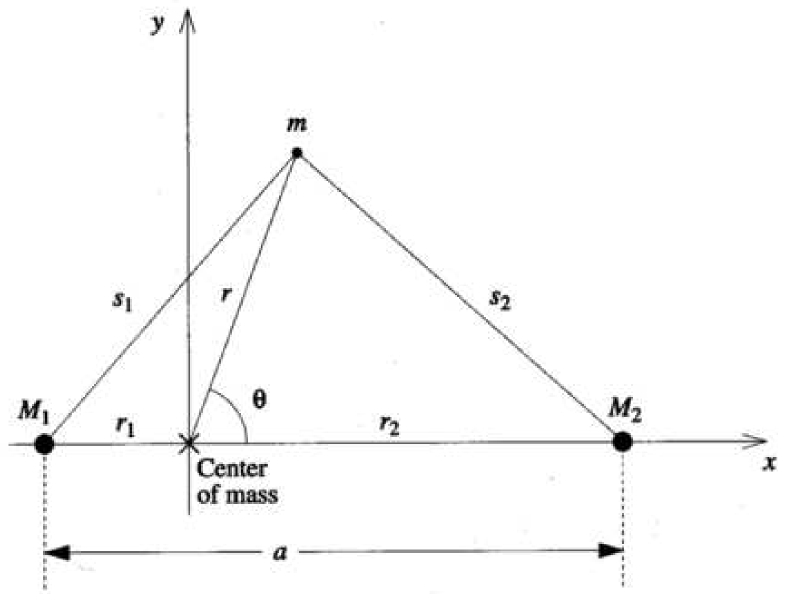

Figure 2.2: Corotating coordinate system with the different distances for a binary system. The vector r marks the position of a test particle. (Figure obtained from Carroll & Ostlie, 1996)

The Roche potential in a binary is determined by the masses of the objects, their distance to each other and their motion around each other. If the center of mass is at the origin, and a corotating coordinate system is chosen, the stars will be at rest in this rotating frame, with their mutual gravitational attraction balanced by the outward 'push' of a centrifugal force (Carroll & Ostlie, 1996, page 684). In the binary frame, assuming a circular orbit, assuming that the stars can be treated as point masses and neglecting the Coriolis force, the Roche potential can be written as

$$\Phi = -\frac{GM_1}{s_1} - \frac{GM_2}{s_2} - \frac{\omega^2 r^2}{2}, \tag{2.1}$$

where s_1 and s_2 are the distances to the center of the stars with mass M_1 and

M_2 respectively; ω is the orbital angular velocity, given by

$$\omega \equiv \frac{2\pi}{P_{\mathrm{b}}} = \sqrt{\frac{G(M_1 + M_2)}{a^3}} \tag{2.2}$$

and r is the distance to the center of mass, $a = r_1 + r_2$ the distance between the two stars (see Figure 2.2) and P_{b} the orbital period.

Points in space that share the same value of Φ form an equipotential sur-

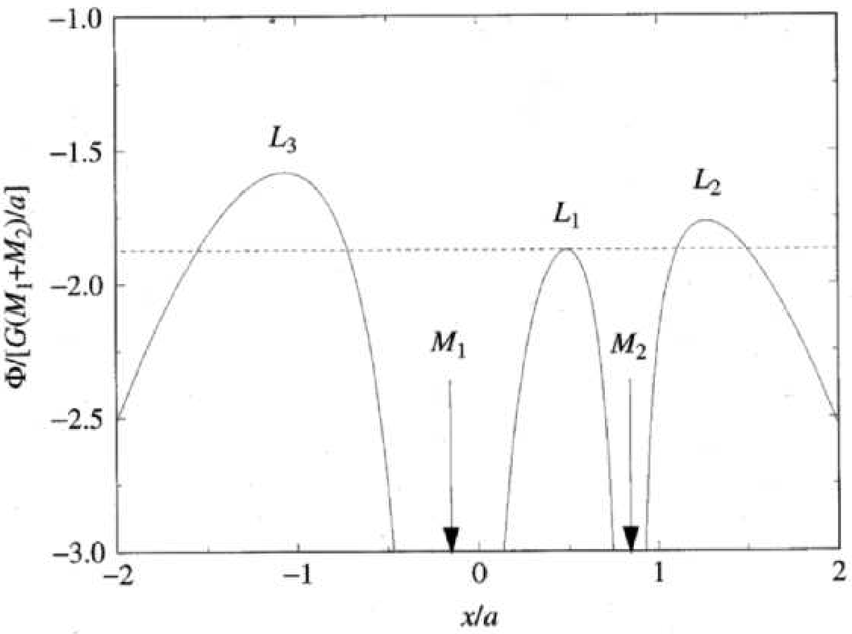

Figure 2.3: The Roche potential Φ along the x-axis, for two stars with a mass ration $q = M_1/M_2 = 5$, with the x-axis through the center of mass and the centers of both stars. The x-axis is in units of a and Φ is in units of $G(M_1 + M_2)/a$. The position of both masses is indicated, and also labeled are the Lagrangian Points (L_1, L_2andL_3) where the combined gravitational potential is balanced by the centrifugal force. The dashed line indicates the value of Φ at the inner Lagrangian point L_1. (Figure obtained from Carroll & Ostlie, 1996)

face. Very close to M_1 or M_2 the equipotential surfaces are nearly spherical and centered on each mass, but farther away the surfaces are distorted into teardrop shapes. When the Roche potential has the level of the inner Lagrangian point (L_1, see Fig. 2.3) both equipotential surfaces around M_1 and M_2 touch each other. These teardrop-shaped regions of space, bounded by this particular equipotential surface are called Roche lobes (Carroll & Ostlie, 1996, pages 686–688). The volume of the Roche lobe around each of the stars can be calculated numerically. Although the Roche lobe will not have the shape of a perfect sphere, the Roche lobe radius can be defined as the radius of a sphere with the same volume as the Roche Lobe. An analytical expression for the Roche lobe radius (around M_2; for the radius around M_1 use $q = M_1/M_2$) is given by Eggleton (1983), valid for all mass ratios

$$R_{\mathrm{L}_2} \approx a\frac{0.49q^{2/3}}{0.6q^{2/3}+\ln(1+q^{1/3})}, \quad \text{with} \quad q = \frac{M_2}{M_1}. \tag{2.3}$$

For values of the potential $\Phi_{\mathrm{L}_1} < \Phi < \Phi_{\mathrm{L}_2}$ the equipotential surface forms a 'dumbbell' around both stars. For even larger values ($\Phi > \Phi_{\mathrm{L}_2}$ or $\Phi > \Phi_{\mathrm{L}_3}$) the equipotential surface is open, and a particle with enough energy can escape through L_2 or L_3 (or through any other point) to infinity.

2.2 Mass transferring Systems

A donor star in a binary system starts transferring mass to its companion when its radius R_{D} is larger than its Roche lobe radius R_{L}, $R_{\mathrm{D}} > R_{\mathrm{L}}$. In general there are three categories of mass transfer, depending on the evolutionary state of the donor star. Case A mass transfer occurs when the donor star is in its hydrogen core burning phase, Case B mass transfer is after the end of central hydrogen burning and Case C mass transfer is after the end of central helium burning.

2.2.1 Mass Transfer Timescales

During the main sequence phase a single star evolves on the nuclear timescale τ_{N}. This timescale is given by the product the available fusable matter in the core with mass M_{core} times the energy per unit mass, ϵ_{N}, divided by the amount of energy that the star loses per unit time, L. This is

$$\tau_{\mathrm{N}} = \frac{M_{\mathrm{core}}\epsilon_{\mathrm{N}}}{L}, \tag{2.4}$$

with $\epsilon_{\mathrm{N}} = 6.3 \times 10^{18}$erg g^{-1} for hydrogen burning.
A main sequence star expands on the nuclear timescale. In a close binary, this may lead to Roche lobe overflow and the onset of mass transfer. During this phase the mass tranfer rate will be of the order of

$$\dot{M}_{\mathrm{trans}} \simeq \frac{M_{\mathrm{env}}}{\tau_{\mathrm{N}}} \tag{2.5}$$

with M_{env} the mass of the envelope of the donor star, but only if it is stable mass transfer, otherwise it will be much higher.
The difference between stable mass transfer and unstable mass transfer depends on the entropy profile of the star, which determines how the star reacts to mass loss, and on the orbital evolution. In general, stars with a radiative envelope

first contract on the dynamical timescale after mass loss to restore hydrostatic equilibrium, next the star expands on the thermal timescale to restore thermal equilibrium. Stars with a convective envelope first expand on the dynamical timescale after mass loss, but thereafter contract on the thermal timescale to restore thermal equilibrium. For a detailed description see Ritter (1996).
If conservative mass transfer, i.e. the total mass and total angular momentum of the system remains constant, takes place from the more massive star to the less massive star, the Roche lobe shrinks. On the other hand, if the mass ratio is reversed, i.e. mass transfer takes place from the less massive star to the more massive star, the Roche lobe grows. These two effects, the radius contraction or expansion of the donor star, and the Roche lobe radius increase or decrease, determines whether the mass transfer will be stable or unstable. Stable mass transfer happens if after exchange of an infinitesimal amount of mass, the donor star remains inside its Roche lobe. Otherwise, if the donor star expands and the Roche lobe radius shrinks, the mass tranfer becomes unstable and runs away (Verbunt, 2000).
After the exhaustion of hydrogen in the core, if the helium core mass exceeds the Schönberg-Chandrasekhar limit, the core contracts on the thermal timescale (also called the Kelvin-Helmholtz timescale, Kippenhahn & Weigert, 1990)

$$\tau_{\mathrm{KH}} = \frac{GM^2}{2RL} \tag{2.6}$$

and on the same timescale the outer layers expand, which means that the mass transfer rate in this phase will be of the order of

$$\dot{M}_{\mathrm{trans}} = \frac{M_{\mathrm{env}}}{\tau_{\mathrm{KH}}}. \tag{2.7}$$

Generally the mass transfer rates during stable case A mass transfer (on the nuclear timescale) are lower than the mass transfer rates during case B (on the thermal timescale). In the context of this thesis Case C mass transfer is not relevant.

2.2.2 Conservative Mass Transfer

The effects of mass transfer on the orbital period and orbital separation are well studied (King et al. 2001 and references therein). In this section analytical formulae will be derived for conservative mass transfer in a binary system.

The orbital angular momentum of a specific stellar object in a binary (with mass M_2) can be written as:

$$J_{\mathrm{M_2}} = M_2 \left(\frac{M_1}{M_1 + M_2} \right)^2 a^2 \omega. \tag{2.8}$$

with M_1 the mass of the other object in the binary, a the orbital separation and ω the orbital angular velocity. From this equation the angular momentum of the orbit is simply the sum of the orbital angular momenta of the objects in the binary, and can be written as:

$$\begin{aligned} J_{\rm b} = J_{\rm M_1} + J_{\rm M_1} &= a^2\omega\frac{M_1 M_2}{M_1+M_2} \\ &= M_1 M_2\sqrt{\frac{Ga}{M_1+M_2}}. \end{aligned} \tag{2.9}$$

In this equation the contribution of the accretion disk and the contribution of the rotation of the two stars to the total angular momentum is neglected.
Taking the derivative of the last equation and dividing by the orbital angular momentum $J_{\rm b}$ gives:

$$\frac{\dot{J}_{\rm b}}{J_{\rm b}} = \frac{\dot{M}_1}{M_1} + \frac{\dot{M}_2}{M_2} + \frac{1}{2}\frac{\dot{a}}{a} - \frac{1}{2}\frac{\dot{M}_1+\dot{M}_2}{M_1+M_2}. \tag{2.10}$$

In the conservative case, all mass lost by one of the stars of the binary is gained by the other:

$$M_1 + M_2 = \text{constant} \Rightarrow \dot{M}_1 = -\dot{M}_2 \tag{2.11}$$

so one can write:

$$\frac{\dot{a}}{a} = 2\frac{\dot{J}_{\rm b}}{J_{\rm b}} - 2\left(1-\frac{M_2}{M_1}\right)\frac{\dot{M}_2}{M_2}. \tag{2.12}$$

Integrating this formula, or rewriting Equation (2.9) for $\dot{J}_b = 0$ (because $J_{\rm b}$ is constant for conservative mass transfer), gives

$$\frac{a_{\rm f}}{a_{\rm i}} = \left(\frac{M_{1,\rm i}M_{2,\rm i}}{M_{1,\rm f}M_{2,\rm f}}\right)^2 \tag{2.13}$$

with $a_{\rm f}$ and $a_{\rm i}$ respectively the final and initial orbital separation, and $M_{\rm i}$ and $M_{\rm f}$ respectively the initial and final mass of one of the components.

2.2.3 Non-Conservative Mass Transfer

In the non-conservative case, the equations become more complicated, because some of the matter is lost to the ISM. Equation 2.11 is therefore rewritten as

$$\dot{M}_1 = -\beta\dot{M}_2 \quad \text{or} \quad \dot{M}_1 + \dot{M}_2 = (1-\beta)\dot{M}_2 \tag{2.14}$$

with M_2 the mass losing star. The mass that is lost from the system will also carry angular momentum away. If we write the specific angular momentum of the mass that is lost as α times the specific orbital angular momentum of the mass-accreting star (i.e. the compact object) we can derive an equation for the loss of angular momentum as

$$\dot{J} = \alpha \underbrace{\left(\frac{M_2}{M_1+M_2}\right)^2 a^2\omega}_{\text{angular momentum per mass unit}} \times \underbrace{(1-\beta)\dot{M}_2.}_{\text{mass lost from the system}} \tag{2.15}$$

This gives, if we divide by $J_{\rm b}$ (Eq. 2.9), the following expression

$$\frac{\dot{J}}{J} = \alpha(1-\beta)\left(\frac{M_2}{M_1+M_2}\right)\frac{\dot{M}_2}{M_1}. \tag{2.16}$$

If no other loss of angular momentum is taken into account, and rewriting Eq. 2.12 with Eq. 2.14, Equation 2.12 may be replaced with

$$\begin{aligned}\frac{\dot{a}}{a} &= -2\frac{\dot{M}_2}{M_2}\left(1-\frac{\beta M_2}{M_1}-\frac{(1-\beta)M_2}{2(M_1+M_2)}\right)- \\ &\quad 2\frac{\dot{M}_2}{M_2}\left(\alpha(1-\beta)\left(\frac{M_2}{M_1+M_2}\right)\frac{M_2}{M_1}\right).\end{aligned} \tag{2.17}$$

King et al. (2001) obtained a similar relation but for the evolution of the orbital period P,

$$\frac{\dot{P}}{P} = -\frac{3\dot{M}_2}{M_2}+\frac{3\dot{M}_2}{M_1}-\frac{2(1-\beta)\dot{M}_2}{M_1+M_2}+3(1-\beta)(\alpha-1)\frac{M_2\dot{M}_2}{(M_1+M_2)M_1} \tag{2.18}$$

which can be written in the form of Eq. 2.17 with Kepler's law. After integrating, in the limit for $\beta \to 0$ (all the matter leaves the system) and $\alpha = 1$ (matter leaves the system with the specific angular momentum of the accretor) they obtained the for the period

$$\frac{P}{P_{\rm i}} = \left(\frac{q_{\rm i}}{q}\right)^3\left(\frac{1+q_{\rm i}}{1+q}\right)^2 e^{3(q-q_{\rm i})} \tag{2.19}$$

with $q = M_2/M_1$, the quantities with the suffix i are the initial values, the quantities without a suffix are the present values.

2.2.4 Critical accretion rate

In Section 2.2.1 we saw that in different evolutionary states the mass transfer rates are different. We were able to give an expression for the mass transfer rate in terms of mass and luminosity. Although this is true within certain margins, the real mass transfer rate will be highly fluctuating.

The mass transfer rate determines highly how binary system with a compact object will appear, i.e. as a transient system or as a persistently bright system

in X-rays. Transient systems have outbursts in X-rays on an irregular time interval for which the mechanism is comparable to the disk instability model in dwarf novae (Wijers, 1996), but are mostly in quiescence, i.e. the donor is visible in the optical (or too dim to be seen) and not outshined by X-rays. It is believed that in nova outbursts an instability in the disk grows, causing the whole disk, or a part of the disk, to fall onto the black hole. This gives rise to a huge increase in luminosity in X-rays. A more detailed description of dwarf novae is given by Smak (1983) and Osaki (1996). Contrary to transient systems, the disk in a persistently bright system is stable, due to the stabilising effect of irradiation, caused by the higher accretion rate onto the compact object.
The transition between persistent behaviour and transient behaviour is given by the critical accretion rate which comes from accretion theory and is currently not very well known for black hole binaries.
The fundamentals of accretion theory are worked out by van Paradijs (1996), King, Kolb & Burderi (1996) and King, Kolb & Szuszkiewicz (1997). Following King et al. (1997) the instability will be suppressed if the whole disk is above the hydrogen ionization temperature ($T_{\rm H} \approx 6500\,$K); the source will thus appear as a persistently bright system. The temperature in the disk itself is determined by the viscous dissipation, i.e. potential energy is converted into heat, which gives an effective temperature

$$T^4_{\rm visc} = \frac{3GM\dot{M}}{8\pi\sigma R^3} \tag{2.20}$$

with M the mass of the central object, $\dot{M}$ the accretion rate, G the gravitational constant, σ the Stefan-Boltzmann constant and R the distance to the central accretor, with $R \gg R_{\rm accr}$ (the radius of the accretor). The second contribution to the temperature in the disk is the irradiation, which is much harder to determine, but King et al. (1997) give the following expression

$$T^4_{\rm irr} = \frac{\eta\dot{M}c^2(1-\beta)}{4\pi\sigma R^2}\left(\frac{H}{R}\right)^2\left(\frac{d\ln H}{d\ln R} - 1\right) \tag{2.21}$$

where η is the efficiency of rest-mass energy conversion into X-ray heating, β the X-ray albedo and $H(R)$ the local disk scale height. The total temperature, determined by the viscous temperature and the irradiation temperature, is now defined by

$$T^4 = T^4_{\rm visc} + T^4_{\rm irr}. \tag{2.22}$$

Since T always decreases with R, the condition $T > T_{\rm H}$ for steady accreation is most stringent at the outer edge $R_{\rm d}$ of the disk (King et al. 1997), therefore the critical accretion rate $\dot{M}_{\rm crit}$ is defined by

$$T(R_{\rm d}) = T_{\rm H}. \tag{2.23}$$

King et al. (1997) derive for the critical accretion rate, i.e. the transition between transient behaviour ($\dot{M} < \dot{M}_{\rm crit}$) and persistent behaviour ($\dot{M} > \dot{M}_{\rm crit}$)

$$\dot{M}_{\rm crit} \simeq 2.86 \times 10^{-11} m_1^{5/6} m_2^{-1/6} P_{\rm h}^{4/3} {\rm M}_\odot {\rm yr}^{-1} \tag{2.24}$$

with $m_1 = M_1/\mathrm{M}_\odot$, $m_2 = M_2/\mathrm{M}_\odot$ and $P_\mathrm{h} = P/\mathrm{hr}$.
Observationally almost all low mass black hole binaries are transient systems, while a huge fraction of the low mass neutron star binaries are persistently bright. This can be explained by the difference in the source of irradiation.
Although the condition for steady accretion is determined at the outer edge of the accretion disk, the source that stabilizes the disk is the irradiation from the inner edge of the disk. Because a black hole has no hard surface it cannot act as a point source for irradiation, as for example a neutron star can do, but in the inner part of the accretion disk, surroundig the black hole, a comparable amount of energy is released, not as a point source, but as a flat surface lying in the disk's central plane (King et al. 1997). This means that the accretion rate for systems with a black hole in the center must be higher than for a system with a neutronstar in its center in order to appear as persistently bright instead of displaying transient behaviour.

2.2.5 The Eddington limit

The mass transfer rate onto a black hole cannot be unlimited, because accretion leads to energy release, mainly at X-ray wavelengths. The luminosity produced by the infalling matter onto a black hole can be estimated by

$$L = \frac{GM_\mathrm{BH}\dot{M}}{R} \sim 0.5\dot{M}c^2 \tag{2.25}$$

with radius $R \sim 2GM/c^2$ for a black hole.
If the outward acceleration due to radiation pressure caused by the X-ray luminosity L_X is larger than the gravitational attraction, matter will be blown away rather than accreted. In equilibrium this gives

$$\frac{L_\mathrm{X}}{4\pi r^2}\frac{\sigma}{c} = \frac{GM_\mathrm{BH}}{r^2}, \tag{2.26}$$

with σ the radiation absorption coefficient, for which in the X-ray regime we may use the Thomson cross section.
The maximum rate at which mass can be accreted onto a compact object is called the Eddington limit (Verbunt 2000)

$$L_\mathrm{Edd} = \frac{4\pi c G M_\mathrm{BH}}{\sigma} = \frac{4\pi c G M_\mathrm{BH}}{0.2 * (1+X)} \tag{2.27}$$

where L_Edd is the Eddington luminosity of the black hole (with mass M_BH), using $0.2 * (1 + X)$ as the opacity coefficient due to electron scattering with X being the hydrogen mass fraction of the accreted material.

2.3 Black Hole Physics

In X-ray binaries the compact object is either a neutron star or a black hole. Because the compact object accretes matter from a disk, the angular momentum

carried by that matter will be added to the central object, causing this object to spin up.
In the theory of general relativity the geometry of rotating compact objects is described by the Kerr-metric, from which the Schwarzschild-metric (no rotation) can be deduced when the Kerr parameter $a = 0$ (Bardeen, 1970).
The Kerr-metric is mostly written (with $G = c = 1$) as (Shapiro et al., 1983)

$$\begin{aligned} ds^2 = &-\left(1 - \frac{2Mr}{\Sigma}\right) dt^2 - \frac{4aMr\sin^2\theta}{\Sigma} + \frac{\Sigma}{\Delta} dr^2 + \\ &\Sigma d\theta^2 + \left(r^2 + a^2 + \frac{2Mra^2\sin^2\theta}{\Sigma}\right)\sin^2\theta d\phi^2 \end{aligned} \tag{2.28}$$

where M is the mass of the black hole, (r, θ, ϕ) the coordinates, $a \equiv J/M$ with J the total angular momentum of the black hole, $\Delta \equiv r^2 - 2Mr + a^2$, $\Sigma \equiv r^2 + a^2\cos^2\theta$.
There is an event horizon if the metric function Δ vanishes. This occurs first at the larger root of the quadratic equation $\Delta = 0$,

$$r_+ = M + (M^2 - a^2)^{1/2}. \tag{2.29}$$

Besides this event horizon three other different radii are important to consider for a rotating black hole, i.e. the last circular photon orbit (r_{ph}), the marginally bound orbit (r_{mb}) and the marginally stable orbit (r_{ms}). The expressions are given by Shapiro & Teukolsky (1983, p. 361–362)

$$\begin{aligned} r_{\mathrm{ph}} &= 2M\{1 + \cos[\frac{2}{3}\cos^{-1}(\mp aM)]\}, && (2.30) \\ r_{\mathrm{mb}} &= 2M \mp a + 2M^{1/2}(M \mp a)^{1/2}, && (2.31) \\ r_{\mathrm{ms}} &= M\{3 + Z_2 \mp [(3 - Z_1)(3 + Z_1 + 2Z_2)]^{1/2}\}, \text{with} && (2.32) \\ Z_1 &\equiv 1 + \left(1 - \frac{a^2}{M^2}\right)^{1/3}\left[\left(1 + \frac{a}{M}\right)^{1/3} + \left(1 - \frac{a}{M}\right)^{1/3}\right], \\ Z_2 &\equiv \left(3\frac{a^2}{M^2} + Z_1^2\right)^{1/2}. \end{aligned}$$

The motion of a particle around a black hole can be prograde (upper sign) or retrograde (lower sign).
For a particle, circular orbits around a black hole are possible from $r = \infty$ to the last circular photon orbit. However, not all the particles in a circular orbit around a black hole are in a bound orbit. Given an infinitesimal outward perbutation, a particle in such an orbit will escape towards infinity, unless the orbit fullfills the condition $r < r_{\mathrm{mb}}$. Note also that r_{mb} is the minimum periastron of all parabolic orbits (Shapiro, 1983). Given a particle that approaches the black hole from infinity, the orbit will be mostly very nearby parabolic, and when it reaches $r < r_{\mathrm{mb}}$ it must plunge into the black hole (Shapiro, 1983). However, for the case of accretion from an accretion disk onto a black hole the matter

slowly loses angular momentum in the disk, until it reaches the last stable orbit ($r_{\rm ms}$). At this point it falls into the black hole, without losing further angular momentum (Bardeen, 1970).
For particles in a circular orbit around a black hole, the specific angular momentum and energy are given by (Shapiro, 1983)

$$\tilde{E} = \frac{r^2 - 2Mr \pm a\sqrt{Mr}}{r(r^2 - 3Mr \pm 2a\sqrt{Mr})^{1/2}}, \tag{2.33}$$

$$\tilde{l} = \pm\frac{\sqrt{Mr}(r^2 \mp 2a\sqrt{Mr} + a^2)}{r(r^2 - 3Mr \pm 2a\sqrt{Mr})^{1/2}}, \tag{2.34}$$

where the upper sign refers to corotating (or prograde) orbits and the lower sign to counterrotating (or retrograde) orbits. This implies that accretion from the last stable orbit adds less angular momentum and energy to the black hole as does accretion from the last bound orbit (see also Brown, 2000). This can also be seen from Fig. 2.4.

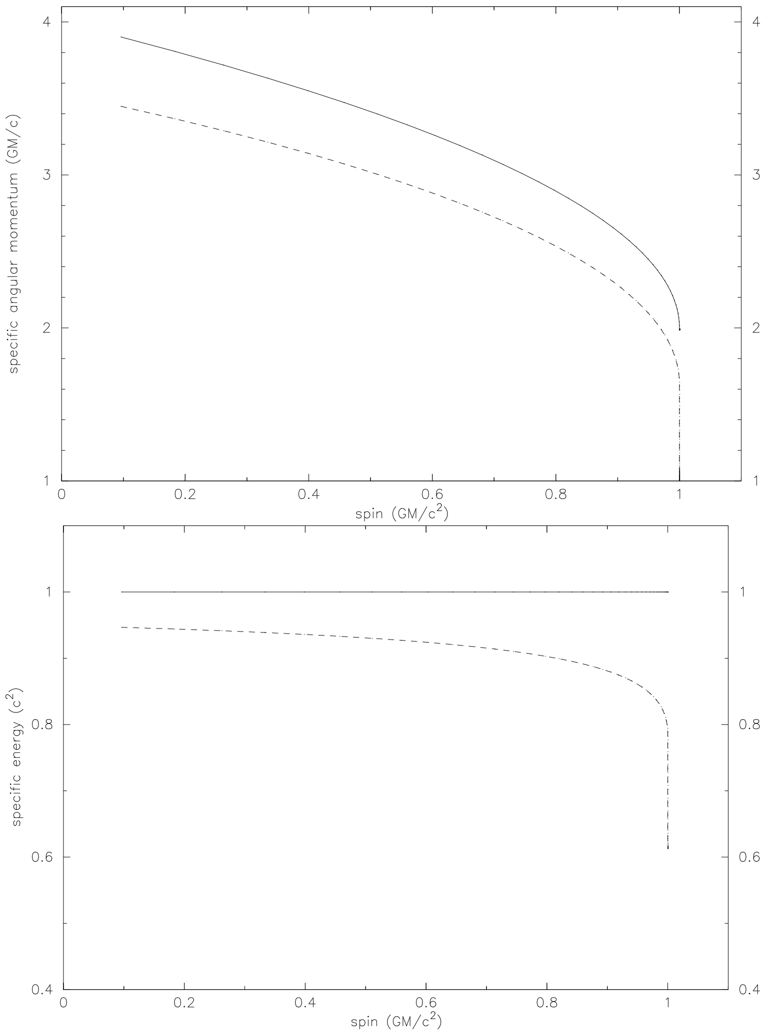

Figure 2.4: Specific angular momentum and energy of test particles in units of $[GM/c]$ and $[c^2]$ as a function of the spin of the black hole a $[GM/c^2]$ for accretion onto the black hole from the last stable orbit (dashed line) and the last bound orbit (solid line).

Chapter 3

The Black Hole Binary System GRO J1655-40

GRO J1655-40 is an X-ray source, discovered in 1994 with the Burst and Transient Source Experiment (BATSE) on board the *Compton Gamma Ray Observatory.* Since then many astronomers have dedicated their attention to this source because there was strong evidence that it could be a black hole binary.
Nowadays there is little doubt about the nature of the primary star; it's a black hole of several solar masses. The mass of the secondary still debated. Since the mass of the secondary has a huge influence on the characteristics of the system, it is worthwhile to finally find the precise mass. It can teach us much about the evolution of this system.
In this chapter I will give an overview of the characteristics of this system, focussing on the observations of both components and the behaviour they display. In the last section some proposed evolutionary models are discussed and I will present my own evolutionary calculations.

3.1 Component Masses

Although several people have tried to fit the lightcurves of the source, there is some discussion about the masses of both objects in the binary. As mentioned above the primary is a black hole of several solar masses.
The observed luminosity ($L = 46.6 \pm 13.6\mathrm{L}_{\odot}$) and temperature ($T_{\mathrm{eff}} = 6500 \pm 250\mathrm{K}$) of the secondary (Orosz & Bailyn 1997) are consistent with a 2.3 $\mathrm{M}_{\odot}$ single star (see Figure 3.1) evolving through the Hertzsprung-gap (Kolb et al. 1997, Kolb 1998). They initially established a mass function of $f(M) = 3.16 \pm 0.15\mathrm{M}_{\odot}$ (Bailyn, 1995) later improved to $f(M) = 3.24 \pm 0.09\mathrm{M}_{\odot}$ (Orosz & Bailyn, 1997). Shahbaz et al. (1999) obtained radial-velocity curves of the system during real quiescence, contrary to Orosz et al. (1997), and found a significantly lower mass function of $2.73 \pm 0.09\mathrm{M}_{\odot}$ using high-resolution spectroscopy. Beer & Podsiadlowski (2002) however, derived on basis of the same lightcurves as Orosz et al.

Table 3.1: Observations of GRO J1655-40. The first column contains the mass of the black hole, the second the mass of the donor star, the third the orbital period in days, the fourth the mass function, the fifth the mass ratio. The second half of the table is in the lower part, with in the first column the luminosity, the second the temperature, the third the radius and the fourth the paper in which the observation is described.

Nr.	$M_{\rm BH}$ $\rm M_\odot$	$M_{\rm D}$ $\rm M_\odot$	P d	$f(M)$ $\rm M_\odot$	$q = M_1/M_2$
1	5.4 ± 0.2	< 1.5	2.601 ± 0.027	3.16 ± 0.15	
2	7.02 ± 0.22	2.34 ± 0.12	2.62157 ± 0.00015	3.24 ± 0.09	2.99 ± 0.08
3	$4.9 - 6.8$	$0.95 - 1.8$	2.62040 ± 0.00098		$3.8 - 5.5$
4	$6.29 - 7.60$	$1.60 - 3.10$			$2.43 - 3.99$
5	$5.5 - 7.9$	$1.7 - 3.3$		2.73 ± 0.09	$2.29 - 2.96$
6	5.4 ± 0.3	1.45 ± 0.35			3.9 ± 0.6

Nr.	L $\rm L_\odot$	T K	R $\rm R_\odot$	paper
1				Bailyn et al. 1995
2	46.6 ± 13.6	6500 ± 250	4.85 ± 0.08	Orosz & Bailyn 1997
3				van der Hooft et al. 1997
4	$31 - 54$			van der Hooft et al. 1998
5				Shahbaz et al. 1999
6	21.0 ± 6.0	6150 ± 350		Beer & Podsiadlowski 2002

(1997) a mass of the secondary corresponding to $1.45 \pm 0.35 \rm M_\odot$ with a luminosity of $L = 21.0 \pm 6.0 \rm L_\odot$ and a temperuature of $T_{\rm eff} = 6150 \pm 350$K and a black hole mass of $5.4 \pm 0.3 \rm M_\odot$. Various other observers (van der Hooft et al., 1997, 1998, and Shahbaz et al., 1999, 2000) have claimed masses for the primary and secondary that lie roughly between the masses of Orosz & Bailyn and Beer & Podsiadlowksi.

3.2 Peculiarities

Some of the information about the nature of the system cannot be obtained from solely the masses, but from the behaviour of the system. In the following we will discuss the transient nature of the system, from which we can say something about the evolutionary state of the secondary, the appearance as a superluminal source from which we can learn about the nature of the primary, and the existence of QPO's and other phenomena that give an indication of the spin of the black hole.

3.2.1 The Transient X-ray Emission

The first idea is, following the previous section, that the luminosity and the temperature of the secondary are most consistent with a star in the hydrogen

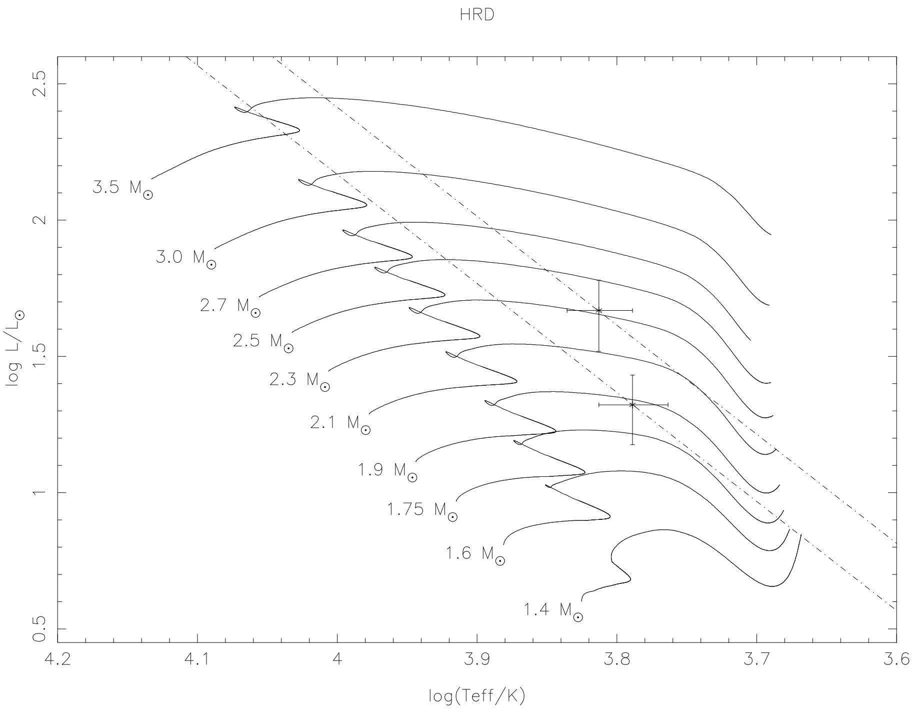

Figure 3.1: Evolutionary tracks in the HR-diagram of 10 single stars ranging from $1.4\mathrm{M}_\odot$ to $3.5\mathrm{M}_\odot$. The tracks start at the zero age main sequence and are continued roughly to the base of the giant branch. They are calculated using the code described in Section 3.3.1. The points with errorbars are from Orosz & Bailyn (1997) - upper point - and Beer & Podsiadlowski (2001) - lower point. The dashed lines are lines of constant radii, respectively $R_2 = 4.05\mathrm{R}_\odot$ and $2.30\mathrm{R}_\odot$).

shell-burning phase (the Hertzsprung Gap). As we will see in Section 3.3.3 the mass transfer rate is much higher than the critical mass transfer rate as expected from Section 2.2.4, what implies that this system would appear as a persistently bright system. Even if the secondary is still on the main sequence (see Section 3.3.2) the mass transfer rate is too large for transient behaviour.

The outbursts themselve are rather atypical. After a period of at least 30 years in quiescence, the system brightened significantly in X-rays at 27 July 1994 (Zhang et al., 1994). The optical counterpart and radio counterpart were identified soon (Orosz et al., 1997). About 3 weeks after the initial hard X-ray outburst, radio jets with apparent superluminal velocities were observed emerging from the source (Orosz et al. 1997, Hjellming & Rupen 1995). The first outburst was followed by two others in late March 1995 and late July 1995 (Esin et al., 2000). In the period between August 1995 and late April 1996 the source was not detected by BATSE (Orosz et al. 1997). This quiescent state ended around April 25, 1996 when a new, soft X-ray outburst began (Esin et al., 2000). The X-ray emission stayed at a rather high value for $\sim$ 200 days. After this outburst the system went back into quiescence until today. Esin et al. (2000) concluded that this last outburst started as a normal X-ray transient outburst. After 27 days a new event occurred which stopped the decline of the X-ray flux and pushed the system for roughly 200 days in a stable state with enhanced mass transfer from the secondary, probably caused by irradiation. Overall they concluded that the mass transfer rate in GRO J1655-40 is close the the stability limit of an irradiated disk, at least during the period directly preceding the 1996 outburst. They estimated this critical mass transfer rate to be about $2 \times 10^{-8} M_{\odot} yr^{-1}$.

At least one feature of the observed behaviour of GRO J1655-40 remains a

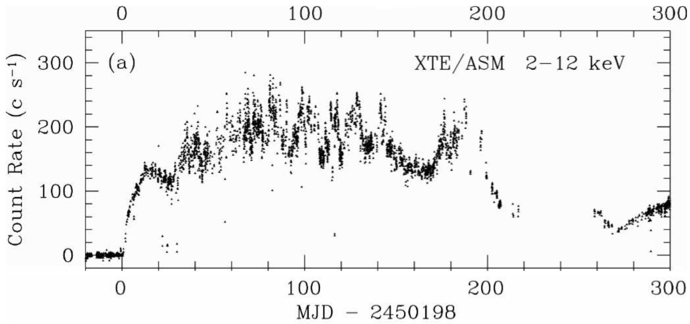

Figure 3.2: X-ray flux during the 1996 outburst. The outburst begins on April 25 (day 0) and 15 days later the maximum luminosity is reached. After $\sim$ 12 days of a roughly exponential decay the source brightens again and reached a strong flaring plateau until day 200. Over the next $\sim$ 70 days the luminosity fell to less than a third of its peak value during the plateau phase. This minimum is followed by a $\sim$ 150 day long reflare, after which the source re-enters quiescence. Figure from Esin et al. (2000).

problem. The recurrence time between the July 1995 outburst and the April 1996 was about 9 months, but before the 1994 outburst the system was at least 30 years in quiescence. How could a system remain so long in quiescence if the mass transfer rate is close to the critical mass transfer rate? Which behaviour is the norm for this system, short periods of quiescence or long periods of quiescence? Esin et al. (2000) choose for the first option but without clear arguments.

3.2.2 Superluminal Outflow

Collimated jets are a common phenomenon in astrophysics. They are often seen in connection to quasars and massive black holes which may power active galactic nuclei. How jets are created is still unkown, but the angular momentum of material moving in a disk around the central object, gives a natural preferred direction for the jets (Hjellming et al. 1995). The distance to quasars and AGN

is too large to see any time variability in the jets within the timescale of some years, or to see some structure in the jets. Relatively nearby objects as the so called micro-quasars, i.e. compact objects with relativistic jets, show time variability of the orders of hours or days and even structures in the jets can be resolved.
As mentioned before, roughly three weeks after the first outburst in X-ray, relativistic jets were seen originating from the central object in GRO J1655-40. Observations with the VLA and VLBA show expanding jets with an escape velocity of $v \geq 0.91c$ (Hjellming et al. 1995). Figure 3.3 show the expanding jets from this source over a time interval of about one month.
The amount of matter lost by the system during the jet-phase is not known, but it is clear that during the 1994 outburst, mass transfer was non-conservative.

3.2.3 Black Hole Spin

Several authors claimed the black hole in GRO J1655-40 to spin at a (nearly) critical spin rate. Four independent arguments for this claim come from the absence of an ultrasoft component in the spectrum, the appearance of superluminal jets, the existence of high-frequency quasi-periodic oscillations (QPO's) and the arguments from the formation of the black hole by a hypernova.

Zhang et al. (1997) argued that systems that contain a fast spinning black hole show an absence of the ultrasoft component of 0.5–1.0 keV in the spectrum during the high luminosity state. They derived that this system most probably contains a Kerr black hole spinning at between 70% and 100% of the maximum rate, with a most likely value of 93% of the maximum rate.

Cui et al. (1998) argued that certain types of quasi-periodic oscillations observed in the lightcurves of black hole binaries are produced by X-ray modulation at the precession frequency of accretion disks, because of relativistic dragging of inertial frames around spinning black holes. From this proposition they derived that the black hole is spinning at 95% of the maximum rate. This claim however is critizised by Abramowicz & Kluźniak (2001) who claims the black hole has a spin between 0.2 and 0.67 of the maximum spin rate, derived from another recently discoved QPO.
In general there is discussion about the interpretation op QPO's and with which physical phenomenon they should be associated.

Lee et al. (2001) described in a recent paper the empirical correlation between the black hole mass and the period of the system. They concluded from this relation that black holes formed in soft X-ray transients acquire a significant Kerr parameter. Using the values for the mass of Beer et al. (2001) they derived, assuming the formation of the black hole by a hypernova, the black hole to be spinning at $0.7 - 0.9$ of the critical spin rate.

In a recent paper Meier (2001) presented a model in which radio-jets are

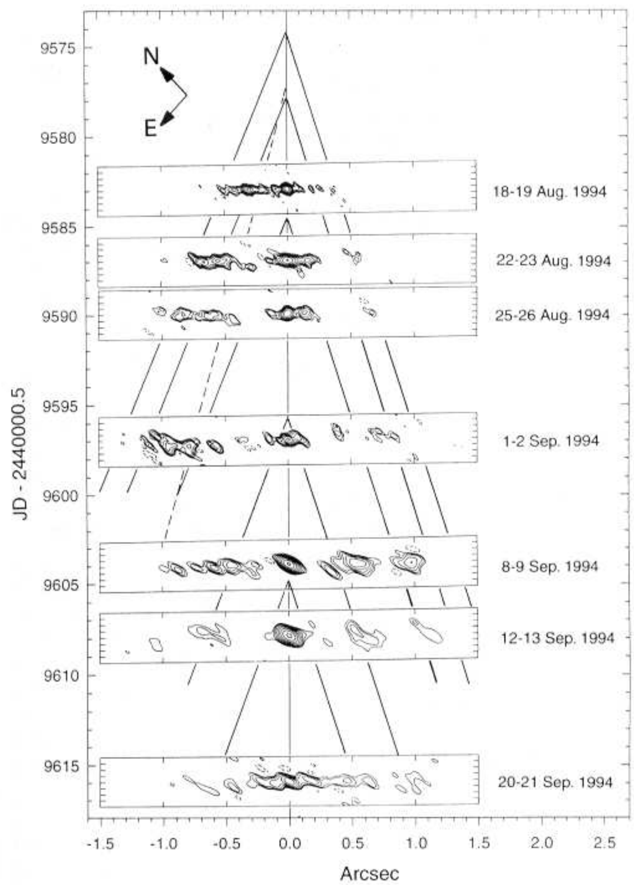

Figure 3.3: A sequence of seven images of GRO J1655-40 taken during the 1994 outburst by the VLBA. The vertical axis represents the time, and the separation of images corresponds to the elapsed time between the images. The horizontal axis gives the spatial offset from the central source marked by the vertical line. Solid lines (time lines) between the images identify motions of 54 mas d^{-1} on the left (NE) and 45.5 mas d^{-1} on the right (SW) side. The dashed line represents the 40 mas d^{-1} fit to the VLA data. Figure from Hjellming et al. (1995).

produced in black hole systems only if the black hole is rapid rotating. Strong evidence for this connection is the fact that jets so far have only been observed in systems which are claimed to spin at (nearly) critical rates, GRO J1655-40 and GRS 1915+105.

3.3 Suggested Progenitor Evolution

Several evolutionary models for the secondary in GRO J1655-40 have been suggested by various authors in the last years. Some of them suggested the secondary to be a Roche lobe filling main sequence star, others think the secondary is a subgiant star filling its Roche lobe. The position of the secondary in the Hertzsprung-Russell diagram is consistent with a star crossing the Hertzsprung Gap (see Fig. 3.1) irrespective of the mass. The evolutionary state of the mass transferring star is highly constrained by the observed quantities of the secondary, i.e. the temperature and the luminosity, but also by the masses of both components and by the observed mass transfer rate that causes the transient behaviour in X-rays. Yet it does not seem to be obvious to construct such an evolutionary model that satisfies all the observed constraints. Below, the different opinions are discussed and some new calculations are presented. In Section 3.3.1 the binary evolutionary code we used to perform the evolutionary calculations is discussed. Section 3.3.2 focusses on the Case A mass transferring systems, while Section 3.3.3 deals with Case B mass transferring systems.

3.3.1 Binary Evolutionary Code

The stellar evolution code we use to calculate our stellar models, is developed by Braun (1997) and is based on an implicit hydrodynamic stellar evolution code for single stars (cf. Langer 1991, 1998). It is a 1-dimensional implicit Lagrangian code which solves the hydrodynamic form of the stellar structure and evolution equations (Kippenhahn & Weigert, 1990). The density ρ, temperature T, radius r, luminosity $L_{\rm r}$ and velocity v are iteratively calculated on the gridpoints $q_{\rm r} = \frac{m_{\rm r}}{M}$ from one timestep to another. The gridpoints are the relative mass coordinates, $M_{\rm r}$ is the mass contained within a radius r, and M is the total mass of the model. The evolution of two stars is calculated simultaneously. Mass loss from the Roche lobe filling component through the first Lagrangian point is computed according to Ritter (1988) as

$$\dot{M} \sim \exp\frac{R - R_{\rm L}}{H_{\rm P}} \tag{3.1}$$

with R the radius of the stellar model, $R_{\rm L}$ Roche radius and $H_{\rm P}$ the pressure scale height. The Roche radius is calculated using the approximation of Eggleton (1983). Mass transfer is assumed to be conservative[1].

The stellar models are computed using OPAL opacities (Iglesias & Rogers, 1996). Changes in the chemical composition are calculated using a nucleosynthesis network of 63 reactions, including the *pp*-chains, the CNO-tri-cycle and the major helium, carbon, neon and oxygen burning reactions.

For all models a metallicity of 2% is adopted. Some models are calculated using convective core overshooting, which is described by Langer (1991) and Braun &

[1]However the superluminal outflows in the form of jets in August and September 1994 imply a non-conservative mass transfer, there is no evidence that, except for this phase, mass transfer was *not* conservative.

Langer (1995). In the models which are computed with overshooting, in most cases overshooting of 0.2 H_P ($\alpha = 0.2$) is applied, with H_P the pressure scale-height.
Further details about the computer code and the input physics can be found in Langer (1998) and Wellstein & Langer (1999).

3.3.2 Case A Mass transfer

The first who suggested that the secondary in GRO J1655-40 could be a main sequence star was van der Hooft et al. in 1998. They derived from new lightcurves an actual mass of the secondary of $2.35 \pm 0.75 M_\odot$ and calculated some progenitor evolution models that could produce this system. Since the secondary is losing mass, it must have evolved from an initially more massive star. As can

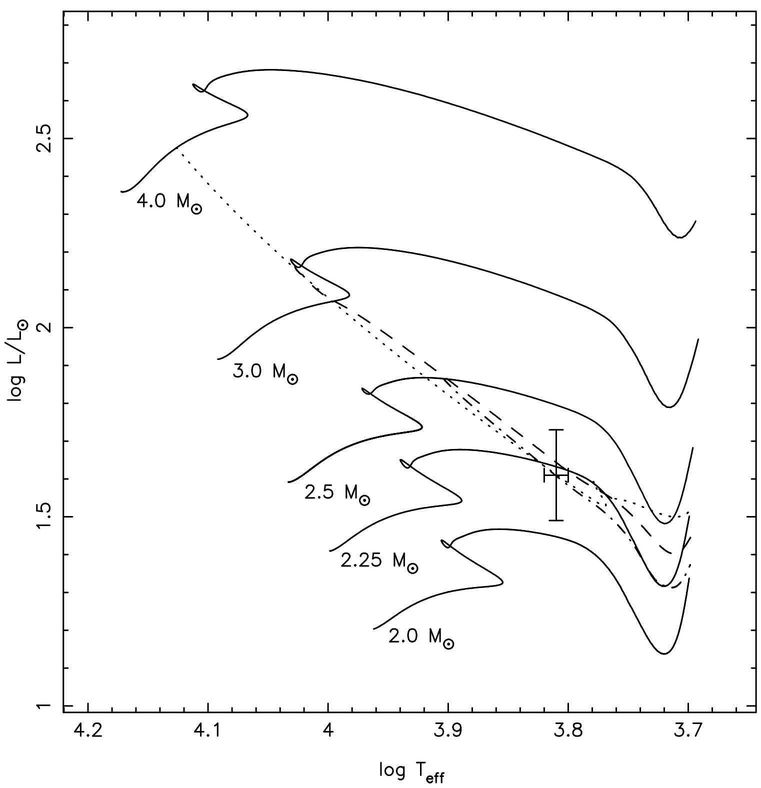

Figure 3.4: The solid lines show evolutionary sequences in the HR-diagram for five single stars of different masses between $2.0M_\odot$ and $4.0M_\odot$. If the same star would have been in a binary system (total mass of $9.2M_\odot$) and filled their Roche lobe, their subsequent evolution is showed with the dashed and dotted lines. The point (with errorbars) is located at the observed luminosity and temperature by van der Hooft et al. (1998). (Figure obtained from van der Hooft et al., 1998)

be seen from Fig. 3.4, stars that are constrained in their orbital evolution by the present orbital period, with a mass around $3.0\mathrm{M}_\odot$ and higher can transfer mass during the main sequence. Detailed evolutionary calculations, however, show that the mass transfer rate is too high to cause transient behaviour of the system.
An example of the evolution of a companion star with a mass of $3.5\mathrm{M}_\odot$ is shown in Figure 3.5. This star fills its Roche lobe during the main sequence,

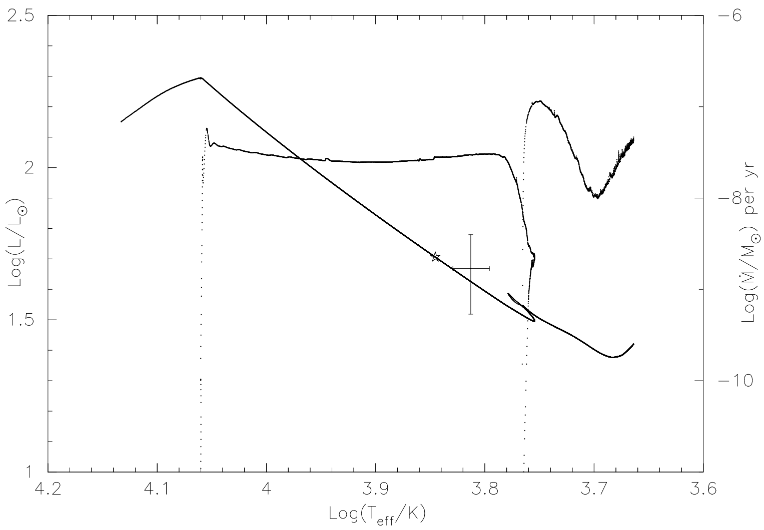

Figure 3.5: The evolutionary sequence in the HRD of a $3.5\mathrm{M}_\odot$-star that fills its Roche lobe during core hydrogen burning. Overplotted is the mass transfer rate (right axis) as a function of the effective temperature. The cross marks the point of the observed luminosity and temperature of Orosz & Bailyn (1997) and the star marks the point where the current period (2.62d) is reached.

and therefore the mass transfer rate remains roughly constant during this phase. The mass transfer rate of $\sim 3\times10^{-8}\mathrm{M}_\odot\mathrm{yr}^{-1}$ is very close to (or above) the critical accretion rate as derived in Section 2.2.4. This critical rate of $M_{\rm crit} \approx 1\times10^{-8}\mathrm{M}_\odot\mathrm{yr}^{-1}$, is derived for a $3.5\mathrm{M}_\odot$ ZAMS-star and a $5.8\mathrm{M}_\odot$-black hole companion, with a period around 1.3d, but this critical rate rises during the subsequent evolution to $\approx 3\times10^{-8}\mathrm{M}_\odot\mathrm{yr}^{-1}$ and is thus marginally consistent with the observed transient behaviour of the source.
In order to get a lower mass transfer rate, we can choose lower masses for the secondary, as the nuclear timescale is longer for these stars and the mass transfer rate thus lower. The conclusion from Figure 3.4 however must be that stars with masses $< 3.0\mathrm{M}_\odot$ are not able to fill their Roche lobe during the main sequence. It is, however, often assumed that a certain amount of convective overshooting should play a role in stars of such masses, which means that the core of the star is enriched with material from just outside the core, causing the star to live

longer. Convective core overshooting also increases the radius of the star (Kippenhahn & Weigert, 1990, 282–284). This implies that even stars with lower masses are able (if the orbital separation is not too large) to fill their Roche lobe during the main sequence, and probably fullfilling the condition that the mass transfer rate should remain below the critical mass transfer rate.
Calculations, based on analytical fitting formulae for stars with overshooting during the main sequence (Hurley et al., 2001), showed that stars more massive than $2.5M_\odot$ are able to fill their Roche lobe. Furthermore, from Fig. 3.6 it

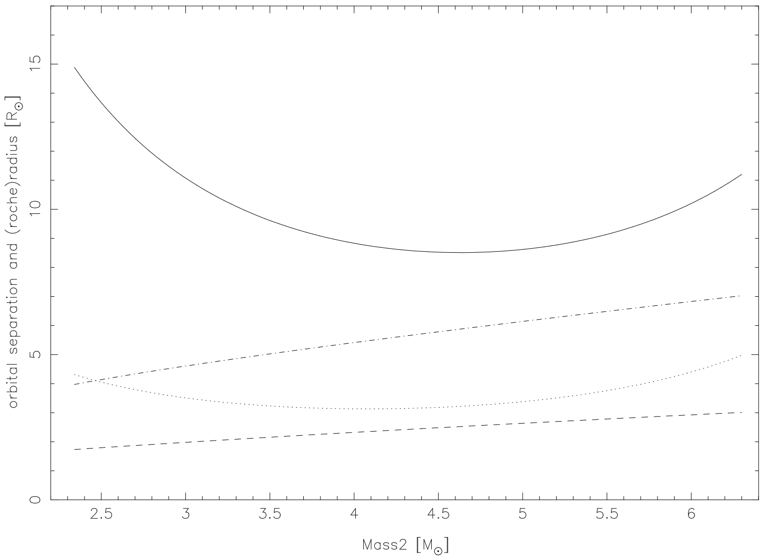

Figure 3.6: The orbital separation, Roche-Radius and the radius of the secondary as a function of the mass of the secondary (with overshooting). Conservative mass-transfer is assumed, hence the mass of the primary and the secondary always sum up to 9.3 $M_\odot$. The solid line gives the orbital separation, the dashed line gives the radius of the secondary at ZAMS, the dash-dotted line gives the radius at TAMS and the dotted line gives the radius of the Roche-lobe. The radius of the secondary at TAMS and the radius of the Roche-lobe are equal if $M_2 = 2.5M_\odot$.

follows that the higher the initial secondary mass, the earlier the mass transfer phase starts, but also that there is a turning point around 4 $M_\odot$ where the Roche radius again gets bigger, caused by the reversed mass ratio q. Assuming that there will not be any black hole less massive than 3 $M_\odot$ the conclusion can be that all stars (with overshooting) with masses between 2.5 $M_\odot$ and ~ 6 $M_\odot$ are able to start mass transfer during their core hydrogen burning phase and can account for the current observed period with conservative mass transfer. However, they cannot all account for accretion rates below the critical accretion rate, as is even the case for stars without overshooting.
Figure 3.7 shows an evolutionary track of a $2.5M_\odot$ star with overshooting ($\alpha = 0.2$) that starts mass transfer during the main sequence. After a short pe-

riod however, the star finishes core hydrogen burning and enters the Hertzsprung Gap and starts its main episode of mass transfer. During this phase, with a high mass transfer rate, it reaches the vicinity of the observed temperature and luminosity. Besides the mass transfer rate which is too high, the period of 2.62d is reached at a too high temperature.

Regős et al. (1998) on the other hand found with a slightly higher secondary

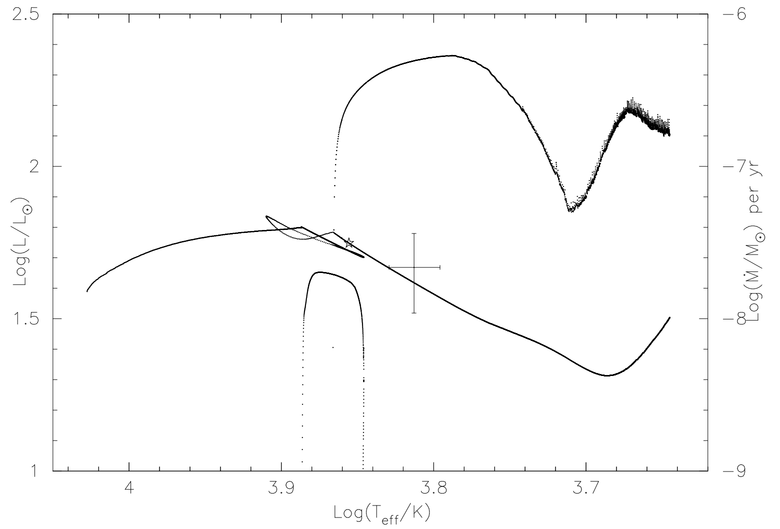

Figure 3.7: The evolutionary sequence in the HRD of a $2.5\mathrm{M}_\odot$-star with overshooting ($\alpha = 0.2$) that fills its Roche lobe during core hydrogen burning. Overplotted is the mass transfer rate (right axis) as a function of the effective temperature. The cross marks the point of the observed luminosity and temperature of Orosz & Bailyn (1997) and the star marks the point where the current period (2.62d) is reached.

mass ($M_2 = 2.75\mathrm{M}_\odot, \mathrm{M}_1 = 6.61\mathrm{M}_\odot, \mathrm{P}_{\mathrm{orb}} = 1.935\mathrm{d}$) an evolution model in which all the quantities seems to fit perfectly, except the point where the secondary reaches $M_2 = 2.34\mathrm{M}_\odot$, and thus the period of 2.62d, is at a too high temperature $\log(T_{\mathrm{eff}}/K) = 3.86$. As can be seen in Fig. 3.8 this is just outside the error bars of Orosz & Bailyn (1997).

It can be concluded from all these attempts to reproduce the observed point of Orosz & Bailyn (1997), that it is possible to reach the vicinity of this point with a star that has initially $2.75\ \mathrm{M}_\odot \lesssim \mathrm{M}_2 \lesssim 3.5\ \mathrm{M}_\odot$, but that there remain problems with the mass transfer rate that is above or close to the critical accretion rate. Because the accretion rate in reality is not a smooth function but probably a highly varying quantity it is reasonable to assume that the real *mean* mass transfer rate is not very close to this critical rate.

New values for the mass of the components in this system from Beer & Podsiadlowski (2001) could solve this problem because their secondary (and primary) have a significantly lower mass, that could account for a much lower mass trans-

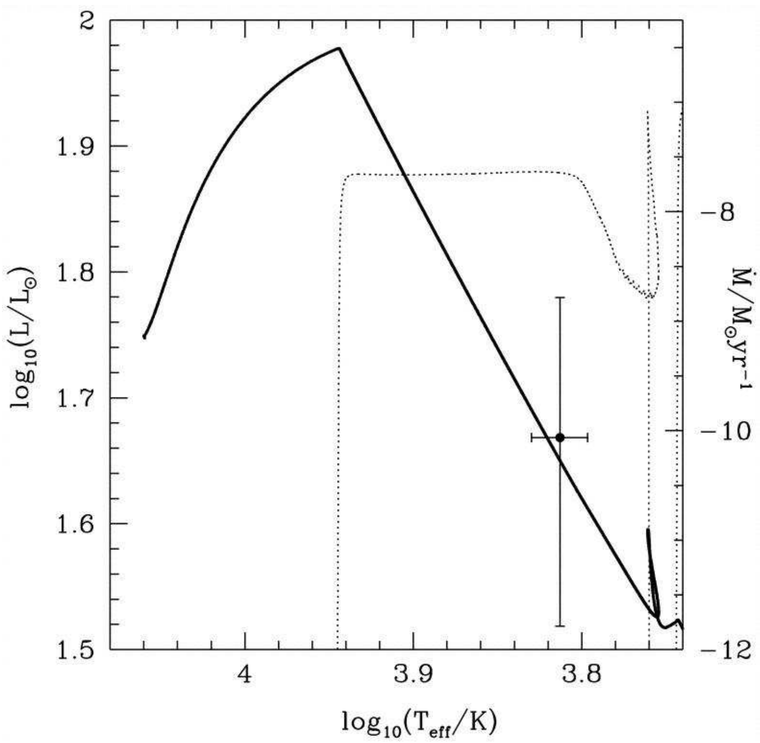

Figure 3.8: Evolutionary sequence of a 2.75 $M_\odot$ star with overshooting that starts mass transfer during the main sequence and reaches the vicinity of the point in the HRD as measured by Orosz & Bailyn (1997). Figure from Regős et al. (1998).

fer rate than the above-mentioned models.

Beer et al. (2001) tried to model the system according to their lower values of the masses (see Figure 3.9), but needed convective overshooting of 0.3 pressure scaleheights (Beer & Podsiadlowski, 2001) and an abundance of 0.7 solar abundance (Podsiadlowski, 2002), with the last requirement the most disputable, since the secondary is significantly polluted by α-elements from the black hole progenitor (Israelian et al. 1999) that should have mixed throughout the entire star. One clear advantage of their model is that they succeeded to remain below the critical mass transfer rate needed for transient behaviour.

An attempt to reproduce the system with the masses obtained by Beer et al. (2001) but without adopting a low metallicity failed. The evolutionary model (see Figure 3.10) goes through the lower error bars of the observed point by Beer & Podsiadlowski (2001) and reaches the observed period just after completing core hydrogen burning and at a temperature far outside the error bars. To correct for the underluminosity the secondary has to start its mass transfer later during the main sequence, but that gives less time to transfer mass and

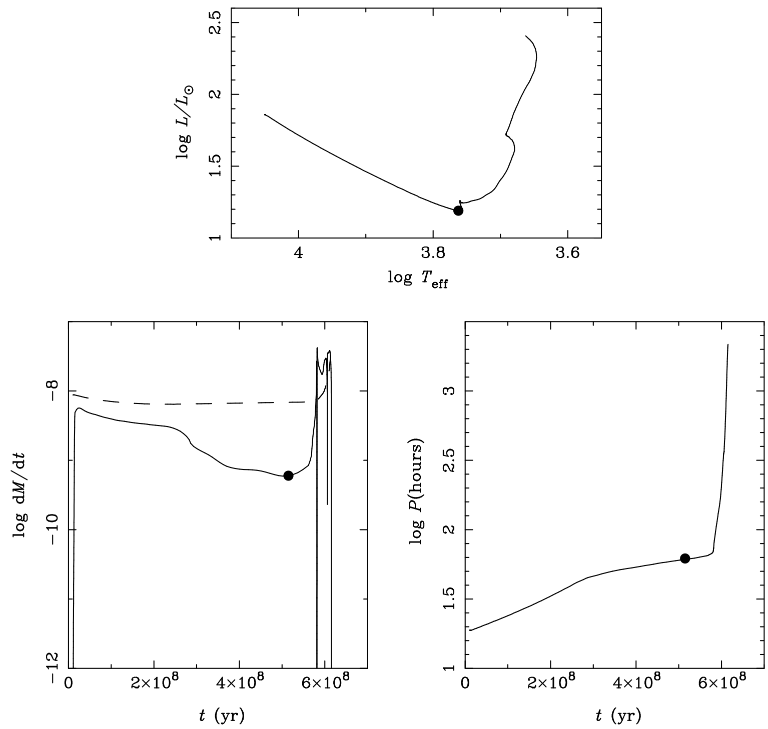

Figure 3.9: Evolutionary sequence of initially a $2.5M_\odot$ secondary and a $4.1M_\odot$ primary leading to the present conditons. The dots indicate the values at the present orbital period (2.6d). The upper panel shows the track in the HRD, the left panel shows the evolution of the mass transfer rate during the main sequence and short thereafter with the dashed curve showing the critical mass transfer rate according (see section 2.2.4), and the right panel shows the evolution of the orbital period. Figure from Beer & Podsiadlowski (2001).

causes the system to reach the currently observed period even later, which is for this model already very difficult to reconcile.

3.3.3 Case B Mass transfer

In Section 2.2.1 we concluded that the mass transfer rate during the hydrogen shell burning phase (Case B) will generally be larger than in case A, because the evolutionary timescale is of the order of the Kelvin Helmholtz timescale, instead of the nuclear timescale which is much longer.
This implies that evolutionary models in which the secondary is somewhere in the Hertzsprung Gap should not be taken too seriously. They all will have mass transfer rates orders too high for transient behaviour of the source. Some authors (Kolb et al. 1997, Kolb 1998) therefore argued that the secondary is in a

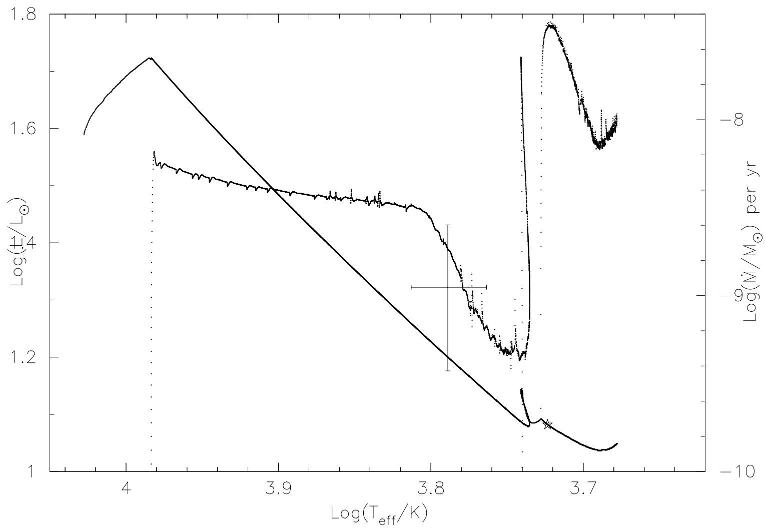

Figure 3.10: Evolutionary model with initial masses of 4.35M$_\odot$ and 2.5M$_\odot$ for respectively the primary and the secondary (with overshooting $\alpha = 0.2$). The star reaches its current period at the position of the star, shorthly after finishing core hydrogen burning. The point with errorbars gives the observed values by Beer & Podsiadlowksi (2001).

special state where transient behaviour is possible. This phase, centered around $\log T_{\rm eff}/{\rm K} = 3.73$, is caused by the transition from thick- to thin-shell source burning (Kolb 1998). Allthough the exact reason is difficult to understand, it is clear that the brief radius contraction, roughly at this temperature, is a feature that is commonly observed in stellar models with masses around 2.5M$_\odot$. The duration and the depth of this phase comes from detailed stellar evolution models, and depend highly on the initial period and on the treatment of convection and opacities (Kolb 1998).
Regős et al. (1998) have tried to model this system, according to the initial masses and period Kolb (1998) derived, but concluded that the phase where the system showed transient behaviour is at a too low temperature, and also that the mass transfer rate almost shuts off in this phase, instead of reaching a level just below the critical accretion rate (see Fig. 3.11).

3.4 Conclusion

In this chapter we looked in detail at the black hole binary system GRO J1655-40. We saw that in the literature there is discussion about the mass of the system, especially the mass of the donor star. Besides that, the evolutionary state of this secondary is not sure. The observed points place the secondary in the middle of the Hertzsprung Gap in the Hertzsprung Russell Diagram. In

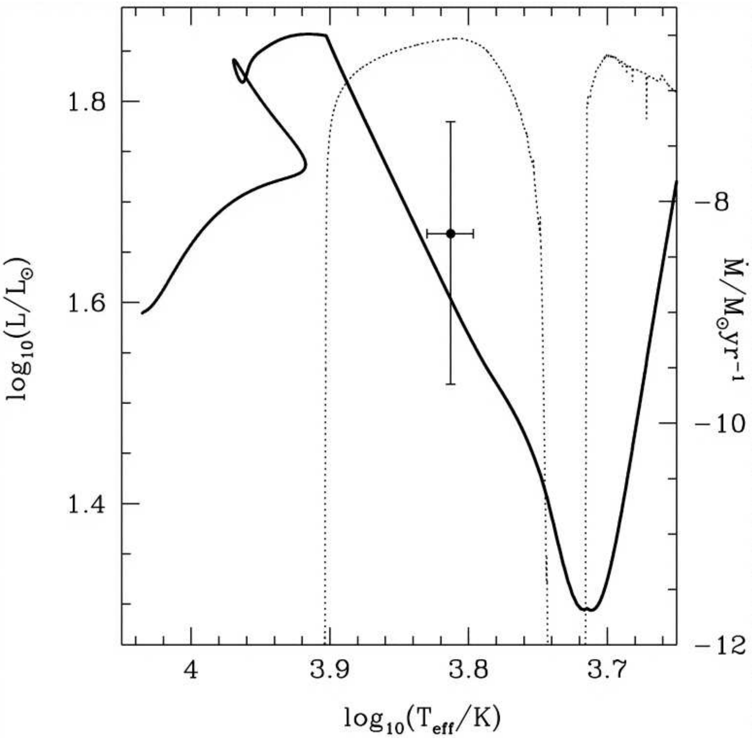

Figure 3.11: Evolutionary model of a 2.5M$_\odot$ star in a binary which starts mass transfer when crossing the Hertzsprung Gap. The dotted line and right-hand scale give the mass transfer rate. The point with errorbars is the observed point by Orosz & Bailyn (1997) At this point the masses of the components are $M_1 = 5.14\mathrm{M}_\odot$ and $M_2 = 1.71\mathrm{M}_\odot$. (Figure from Regős et al. (1998))

this phase the star burns hydrogen in a shell and the star thus undergoes Case B mass transfer if the Roche lobe is filled. Detailed evolutionary calculations, however, show that the mass transfer rate during this phase is much too high to form a transient system. Case B evolution is therefore unlikely. Our focus was therefore on Case A evolution.

Evolutionary models for two different masses of the donor star (2.30M$_\odot$ and 1.45M$_\odot$) were investigated. Taking into account the orbital evolution and the evolution of the star itself, we can conclude that the secondary, with a mass of 2.30M$_\odot$ as measured by Orosz & Bailyn (1997), could be formed from an initially 2.75M$_\odot$ star. In these calculations we need some amount of overshooting. The present star should be near the end of core hydrogen burning. From the calculations it follows, however, that the mass transfer rate is quite close to the critical mass transfer rate of $\sim 2 \times 10^{-8}$ M$_\odot$yr^{-1}.

Our attempts to calculate an evolutionary model for the secondary mass as

observed by Beer & Podsiadlowski (2002) failed, since the constraints on the period are too tight.
We also reviewed some results in the literature about the peculiarities of this system, in the hope to obtain some constraints on the evolutionary status of the system. From the transient X-ray emission we can conclude that the mass transfer rate is close to, but below the critical mass transfer rate, which is estimated at 2×10^{-8} $M_{\odot}yr^{-1}$. From the superluminal outflow which occured in the summer of 1994 in the form of two jets, we can conclude that the system had at least one episode of non-conservative mass transfer, but the amount of matter lost is not well known. The spin of the black hole could give a nice constraint on the evolution of the system, because we approximately know how a black hole is spun up. Observations of the spin of the black hole in GRO J1655-40 show that the black hole is spinning, but the estimates of the rate are divergent.

Chapter 4

Generalized Main Sequence Star Models

Under the assumption that the secondary in GRO J1655-40 is a main sequence star we want to investigate if there are mass-luminosity relations that can fit real evolutionary tracks, not only for single stars without mass loss, but also for stars in a binary with mass loss. At first we will investigate the mass-luminosity-relations derived by Kippenhahn & Weigert that are used as standard relations for main sequence stars. Although these relations are commonly used, the underlying assumptions are not always suitable in all situations, and some adaptations are needed, as shown in this chapter. The remaining part of this chapter is devoted to a new method that uses artificially created stellar models to obtain an accurate Mass-Mean Molecular Weight-Luminosity relation, and to compare this relation with realistic stellar evolutionary models of single stars and stars with mass loss.

4.1 Mass-Luminosity Relations

For main sequence stars it is possible to obtain solutions of stellar models by simple transformations. These transformations are based on homology, the similarity between different solutions, which need however severe conditions that real stars almost never match (Kippenhahn & Weigert, 1990). In this section the homology relations and the mass-luminosity relation obtained by Kippenhahn & Weigert are summarized in brief. In Section 4.1.2 some generalisations of the mass-luminosity relations are discussed and in Section 4.1.3 empirical mass-luminosity relations are discussed.

4.1.1 Homologous Stars

We will derive the homology relations by comparing two homologous stars of masses M and M' with different chemical compositions, represented by the mean molecular weight μ and μ', that are supposed to be homogeneous. The ratios of these two basic parameters are called

$$x = M/M' \text{ and } y = \mu/\mu' \tag{4.1}$$

We now write the basic variables radius, pressure, temperature and luminosity (resp. r, P, T and l), supposing that they are proportional in different models to each other, as the ratios

$$\frac{r}{r'} = z = \frac{R}{R'}; \qquad \frac{p}{p'} = p = \frac{P}{P'}; \qquad \frac{T}{T'} = t = \frac{T_c}{T_c'}; \qquad \frac{l}{l'} = s = \frac{L}{L'}. \tag{4.2}$$

and we will write these ratios as a powerlaw dependend on the mass and the mean molecular weight, with the exponents to be calculated later

$$z = x^{z_1} y^{z_2}; \qquad p = x^{p_1} y^{p_2}; \qquad t = x^{t_1} y^{t_2}; \qquad s = x^{s_1} y^{s_2}, \tag{4.3}$$

The assumptions under which these expressions are justified could be found in Kippenhahn & Weigert (1990, Pages 192–193).
In order to relate these expressions for the basic variables to the material functions, we write

$$\rho \sim P^{\alpha} T^{-\delta} \mu^{\varphi}, \qquad \epsilon \sim \rho^{\lambda} T^{\nu}, \qquad \kappa \sim P^{a} T^{b} \tag{4.4}$$

Kippenhahn & Weigert (1990, page 193–194) obtained, after some algebra, expressions for the exponents in Eq. 4.3

$$\begin{aligned} z_1 &= \frac{1}{2}(1+A), \qquad p_1 = -2A, \qquad t_1 = \frac{1}{2\delta}[1 + (3-4\alpha)A] \\ s_1 &= 1 + \frac{4-b}{2\delta} + \left[2 + 2a + \frac{3-4\alpha}{2\delta}(4-b)\right] A, \text{ and} \end{aligned} \tag{4.5}$$

$$\begin{aligned} z_2 &= \varphi B, \qquad p_2 = -4\varphi B, \qquad t_2 = \frac{\varphi}{B}[1 + (3-4\alpha)B] \\ s_2 &= \frac{\varphi}{\delta}(4-b) + \varphi\left[4 + 4a + \frac{3-4\alpha}{\delta}(4-b)\right] B, \text{ with} \end{aligned} \tag{4.6}$$

$$A = \left[\frac{4\delta(1+a+\lambda\alpha)}{\nu+b-4-\lambda\delta} + 4\alpha - 3\right]^{-1}, \qquad B = A\left(1 - \frac{\lambda\delta}{\nu+b-4}\right)^{-1} \tag{4.7}$$

One of the simplest approximations to fit some properties of main sequence stars is with the approximation of ideal gas ($\alpha = \delta = \varphi = 1$) and constant opacity ($a = b = 0$). This gives with Eqs. 4.5 –4.6 the surprisingly simple result

$$\frac{L}{L'} = \left(\frac{M}{M'}\right)^3 \left(\frac{\mu}{\mu'}\right)^4 . \tag{4.8}$$

This means that in a star of an ideal gas, with constant opacity, the luminosity is not related to the modes of energy generation (i.e. *pp*-chain or CNO-cycle), but is only determined by hydrostatic equilibrium and radiative energy transfer (Kippenhahn & Weigert, 1990, page 195). One important remark is that this relation is only valid for chemically homogeneous stars.

4.1.2 Generalisations

The assumption of chemical homogeneity is one of the basics of the homology relations. In order to obtain more accurate mass luminosity relations, we therefore cannot adopt other chemical compositions, but should seek for other possibilities. In the two next paragraphs two other possibilities are investigated, i.e. the Kramers opacity that uses different exponents in the expression for the opacity (Eq. 4.4) and the contribution of radiation pressure to the ideal gas law.

Kramers Opacity

For the very simple mass luminosity relation of Eq. 4.8 a constant opacity is used. It is not likely that the opacity throughout the star is always constant. A classical approximation for the opacity is given by the Kramers opacities, which has the form

$$\kappa \sim \rho T^{-7/2} \tag{4.9}$$

with κ the opacity, ρ the density and T the temperature. With these approximations, the exponents s_1 and s_2 are now dependent on the energy generation ($\nu \approx 4..5$ for the *pp*-chain and $\nu \approx 15..18$ for the CNO-cycle). The exponents for the different energy generation modes and temperature sensitivity are given in Table 4.1. The effect of the Kramers opacity is plotted, combined with the effects of radiation pressure in Fig. 4.2.

Table 4.1: Exponents in Eq. 4.3 for various temperature sensitivities ν of the nuclear reactions, and for $\alpha = \delta = \varphi = 1$, $a = 1, b = -7/2$, and $\lambda = 1$.

ν:	4	5	15	18
s_1	4.60	4.65	4.84	4.86
s_2	7.27	7.35	7.70	7.74

Radiation Pressure

The pressure inside the star is not only determined by the pressure of the gas, because also photons can contribute significantly to the pressure. Deep inside the star, but also in the outer layers, the radiation is almost equal to black body radiation, which means that its pressure $P_{\rm rad}$ is given by (Kippenhahn & Weigert, 1990, page 104)

$$P_{\rm rad} = \frac{1}{3}u = \frac{a}{3}T^4 \tag{4.10}$$

where u is the energy density and a is the radiation density constant $a = 7.56464 \times 10^{-15}$erg cm^{-3}K^{-4}, which gives for the total pressure

$$P = P_{\rm gas} + P_{\rm rad} = \frac{\Re}{\mu}\rho T + \frac{a}{3}T^4. \tag{4.11}$$

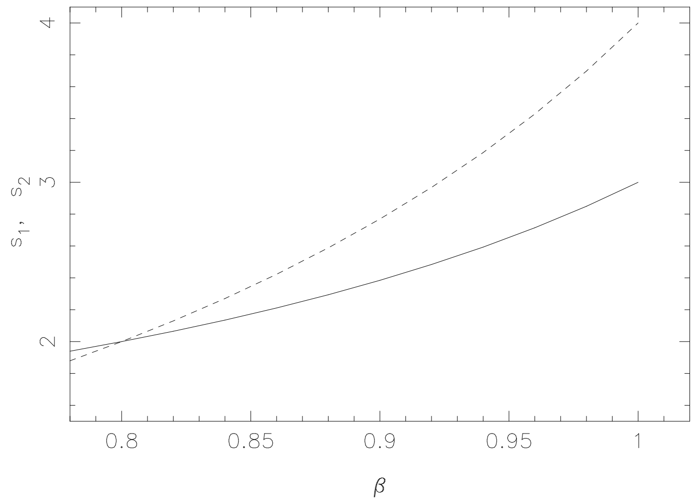

Figure 4.1: This figure shows the effect of the radiation pressure, as measured with β, on the exponents of the mass s_1 (the solid line) and s_2 (the dashed line) in a star with constant opacity ($a = b = 0$). If radiation pressure is not important ($\beta = 1$) the exponents have the value of 3 and 4 resp., as is the case for an ideal gas. If the radiation pressure becomes more dominant the exponents get smaller, i.e. a less steep dependence of the luminosity on the mass and the mean molecular weight. There is no effect of the mode of energy generation.

Following Kippenhahn & Weigert (1990) we can define a measure for the importance of the radiation pressure by

$$\beta := \frac{P_{\rm gas}}{P}, \qquad 1 - \beta = \frac{P_{\rm rad}}{P}. \tag{4.12}$$

For $\beta = 1$ the radiation pressure is zero, while $\beta = 0$ means that the gas pressure is zero.
If we write Eq. 4.11 in the form $\rho \sim P^\alpha T^{-\delta} \mu^\varphi$ we obtain

$$\alpha = \frac{1}{\beta}, \qquad \delta = \frac{4 - 3\beta}{\beta}, \qquad \varphi = 1. \tag{4.13}$$

These exponents can be substituted into Eqs. 4.5–4.6 to obtain new values for the exponents in the mass-luminosity relation. Since the ratio of the radiation pressure to the total pressure is not constant throughout the star, the exponents *alpha* and *delta* will also vary, and thus limit the accuracy of this mass-luminosity relation.
In Figure 4.1 the value of the exponents (s_1 and s_2) are shown for the case of constant opacity ($a = b = 0$). Because of the fact that the square brackets in the equations for s_1 and s_2 vanish, the exponents have no ν-dependence anymore, and this plot thus holds for both the *pp*-chain ($\nu \approx 4...5$, here fixed at 4.5) and

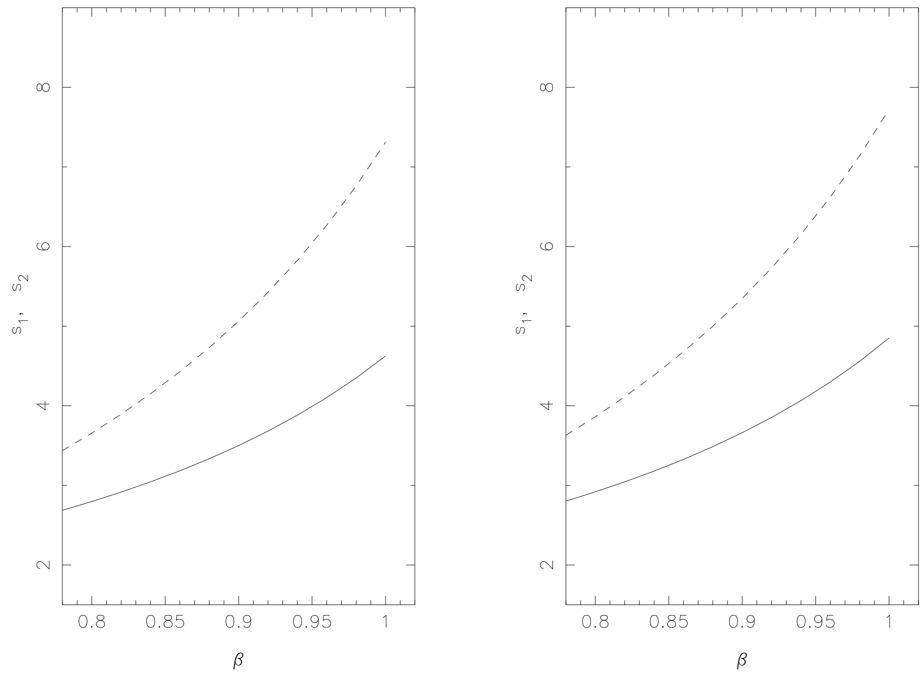

Figure 4.2: This figure shows the effect of the radiation pressure, as measured with β, on the exponents of the mass s_1 (the solid line) and s_2 (the dashed line) in a star with Kramer's opacity ($a = 1.0, b = -7/2$). The left panel is for energy generation in the *pp*-chain ($\nu = 4.5$) and the right panel for energy generation in the CNO-cycle ($\nu = 16.5$). If the radiation pressure becomes more dominant the exponents get smaller, i.e. a less steep dependence of the luminosity on the mass and the mean molecular weight.

the CNO-cycle ($\nu \approx 15...18$, here fixed at 16.5). If the radiation pressure increases, the dependence of the luminosity on the mass and the mean molecular weight gets less steep.

Combining the approximation of radiation pressure with the approximation of the Kramer's opacity ($a = 1.0, b = -7/2$), these will probably better match reality than a constant opacity throughout the star. Figure 4.2 shows the dependence of the exponents on the radiation pressure and the energy generation mode. It is interesting to note that the values of s_1 and s_2 are much higher, especially when there is no effect of radiation pressure ($\beta = 1$).

4.1.3 Empirical Mass-Luminosity Relations

Chemically homogeneous, hydrogen burning models, in thermal and hydrostatic equilibrium, can be easily calculated and can give a view of the zero-age main sequence. Using stars in binaries (for which the mass can be measured very accurately), we can compare these models with real stars, that are supposed to be on or near the zero-age main sequence. When the stars evolve along the main sequence, their luminosity will increase. Figure 4.3 shows the mass luminosity relation for zero-age main sequence models with overplotted observed main sequence double stars. This relation can be fitted with

$$L \sim M^{\eta}. \tag{4.14}$$

As can be seen the slope of the $M - L$ relation varies with M. Over the whole mass range the average of η is about 3.2. For $M = 1...10\mathrm{M}_{\odot}$ the average exponent is 3.88, while in the larger range $M = 1...40\mathrm{M}_{\odot}$ it is 3.35 (Kippenhahn & Weigert, 1990, page 209). The decreasing slope toward higher M is an effect of the increasing effects of radiation pressure.

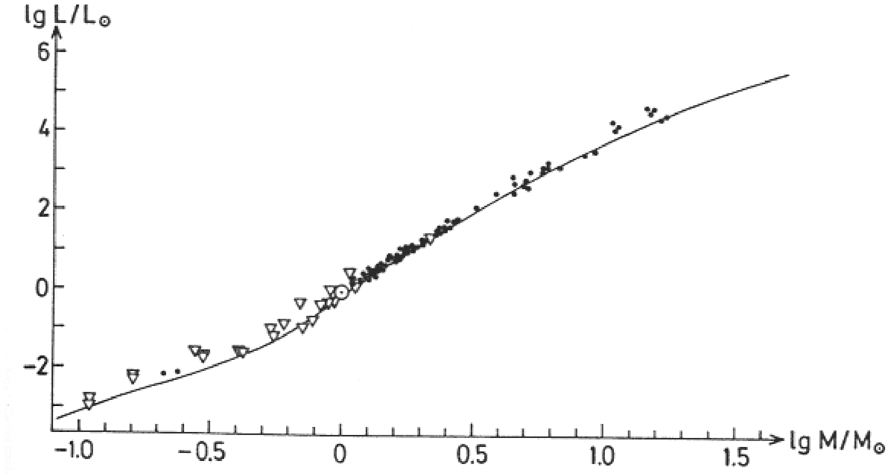

Figure 4.3: The line shows the mass-luminosity relation from ZAMS-models with $X_{\mathrm{H}} = 0.685$, $X_{\mathrm{He}} = 0.294$. The dots are the best measurements (as selected by Popper, 1980) of main-sequence components in detached binary systems and the triangles are of visual binary systems. The position of the sun is indicated by $\odot$. (Figure from Kippenhahn & Weigert, 1990).

4.2 Simplified Numerical Models

According to the Vogt-Russell theorem, the mass and composition of a star uniquely determine its radius, luminosity, and internal structure, as well as its subsequent evolution (Carroll & Ostlie, 1996, Page 368). As we saw in the previous sections, for main sequence stars there are also mass luminosity relations.
During the main sequence the mean molecular weight in the core changes due

to hydrogen buring. This implies, because fusion processes only act in the core of the star, that the mean molecular weight is no longer constant throughout the star.
The aim of this section is to derive a mass luminosity relation that is useful during the entire period that a star is on the main sequence, and that could deal with stars that are no longer chemical homogeneous.
We therefore define the average mean molecular weight $\bar{\mu}$ as the mean molecular weight averaged over the mass

$$\frac{1}{\bar{\mu}} = \frac{1}{M} \int_{m=0}^{M} \frac{1}{\mu(m)} \mathrm{d}m \tag{4.15}$$

with $\mu(m)$ the local mean molecular weight, m the Lagrangian mass coordinate and M the total mass. It could also be defined as an average over the radius or the pressure, but it is superior to averaging over r or P in that it is invariant to structural changes that leave the composition profile intact, whereas other ways of averaging are not. We will see in Section 4.3 that this choice results in a mass luminosity relation that is in good agreement with detailed models.

4.2.1 The L-M-$\bar{\mu}$ - plane

We start with a chemically homogeneous model (ZAMS model). For the mass inside the ZAMS convective core we decrease the central hydrogen abundance $X_{\rm c}$ in a number of models and let the star relax into thermal and hydrostatic equilibrium. In this way we approximate the subsequent evolutionary states along the main sequence.
Two effects, which presumably will have an effect on the luminosity of the star, are not taken into account in this method. The first is the fact that the convective core shrinks during the evolution along the main sequence. The second effect, related to the first, is the steep transition between the core and the envelope, which will be a smooth transition in detailed stellar evolutionary models. These two effects will limit the accuracy of the results.

With the luminosity L determined by two variables, the mass M and the average mean molecular weight $\bar{\mu}$ we can construct a surface in the $M - \bar{\mu} - L$-space. This surface can be described by the following expression, in which the exponents have to be determined later,

$$L \sim M^{\alpha} \bar{\mu}^{\beta}, \text{or} \qquad \left(\frac{L}{\mathrm{L}_{\odot}}\right) \sim \left(\frac{M}{\mathrm{M}_{\odot}}\right)^{\alpha} \bar{\mu}^{\beta}. \tag{4.16}$$

To construct this surface we calculated 220 different artificial stellar models that are all relaxed into hydrostatic equilibrium and thermal equilibrium. The energy generation, needed for these equilibria is taken into account, but no chemical changes are allowed in the core during the relaxation phase.
The artificial stars are calculated for 22 masses (1.00, 1.05, 1.10, 1.15, 1.20,

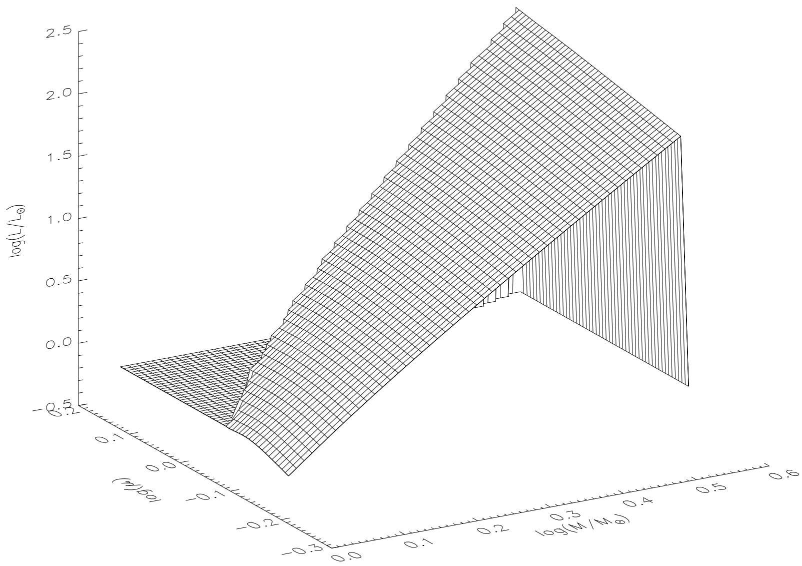

Figure 4.4: The luminosity, $\log(L/\mathrm{L}_{\odot})$ as a function of the mass, $\log(M/\mathrm{M}_{\odot})$ and the average mean molecular weight $\log\bar{\mu}$. As can be seen the surface is not a completely flat surface, which means that the approximation of a powerlaw is not completely justified.

1.30, 1.40, 1.50, 1.60, 1.70, 1.80, 1.90, 2.00, 2.10, 2.20, 2.30, 2.40, 2.50, 2.60, 2.80, 3.00 and $3.25\mathrm{M}_{\odot}$). For each mass ten different models have been calculated with different hydrogen abundances in the core ($X_{\mathrm{c}} = 0.70$, 0.62, 0.55, 0.47, 0.39, 0.32, 0.24, 0.16, 0.085 or 0.008), giving ten different values of the average mean molecular weight. These values of the average mean molecular weight are different for each mass because of the different ratio of the core mass to the total mass.

The grid, determined by the different masses and $\bar{\mu}$, that gives rise to the luminosity-surface is shown in Figure 4.5. Single stars that do not undergo mass loss are expected to stay in this plane. The evolution of a single star, without mass loss, starts at the lower axis (at $\bar{\mu} = 0.617$) and with increasing time, and thus increasing helium abundance in the core, the average mean molecular weight increases, causing the star to move upward.

The discontinuity in the chemical profile, i.e. the steep increase in hydrogen abundance just outside the core, is fixed for each mass at the mass of the ZAMS-convective core. This means that for terminal-age main sequence mod-

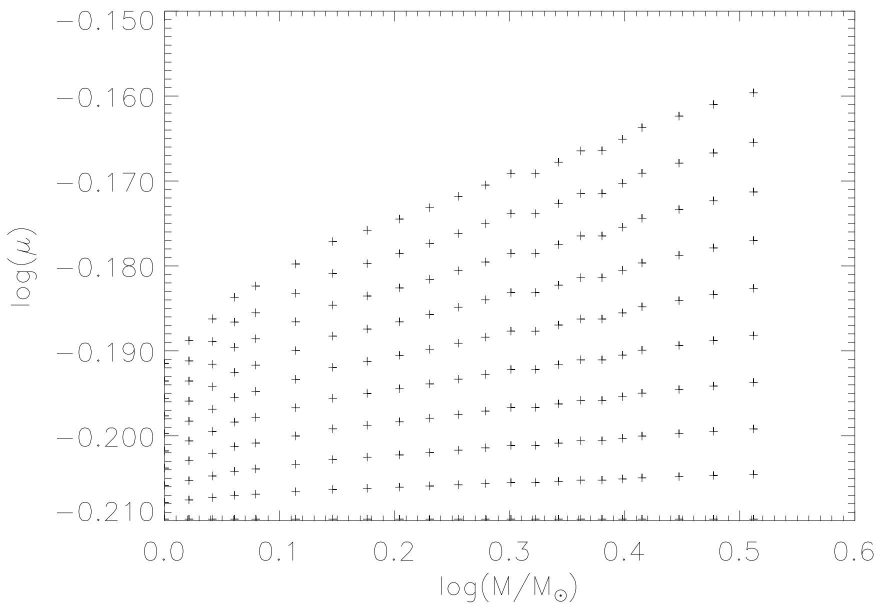

Figure 4.5: The plane of $\log(M/\mathrm{M}_\odot)$ and the average mean molecular weight $\log\bar{\mu}$ in which the 220 computed artificial stars lie. The artificial stars are calculated for 22 masses, ranging from 1 $\mathrm{M}_\odot$ to 3.25 $\mathrm{M}_\odot$. For each star of a certain mass there are ten different values of the Hydrogen abundance in the core, giving ten different values of the average mean molecular weight.

els (TAMS) the discontinuity is outside the actual convective core because the core has shrunk significantly during the main sequence. The terminal age main sequence will therefore not coincide with the upper 'boundary' in Figure 4.5, because these models have a too large value of the average mean molecular weight due to their relatively large core compared to the total mass. From a comparison with detailed single star evolutionary models (see Section 4.3.1) we conclude that the line of the terminal age main sequence is roughly at the second-before-the-last model.

To obtain the exponents in Eq 4.16 the surface is fitted with a modified[1] version of the Downhill Simplex Method (Press et al., 1992, page 402–406). Fitting this surface gives

$$\log\frac{L}{\mathrm{L}_\odot} = 1.08 + 4.03\log\frac{M}{\mathrm{M}_\odot} + 5.27\log\bar{\mu} \tag{4.17}$$

[1] by Cees Bassa, bassa@astro.uu.nl

or

$$\frac{L}{\mathrm{L}_\odot} = 12.02 \frac{M}{\mathrm{M}_\odot}^{4.03} \bar{\mu}^{5.27}. \tag{4.18}$$

The surface is not fitted on the entire grid, because of the deviating behaviour around $1.0\mathrm{M}_\odot$, as can also be seen in the observed $L-M$-diagram (see Fig. 4.3). Also the last two gridpoints for each mass (with the lowest hydrogen abundance in the core) are excluded from the fit, because of the different behaviour of a star with such a low hydrogen abundance in the core and the fact that the terminal age main sequence, according to detailed single star evolutionary models without mass loss, does not extend to such high values of the average mean molecular weight.
We expect that this $M-L-\bar{\mu}$ relation holds for main sequence stars as well as for stars with mass loss, and is thus useful for binary calculations. The difference between the original surface of the artificial stars and the surface with the fitted exponents is showed in Fig. 4.6. As can be seen the differences are very small (<5% for the masses between 1.25 $\mathrm{M}_\odot$ and 3.25 $\mathrm{M}_\odot$), implying that the fit is of a high accuracy in this mass range.

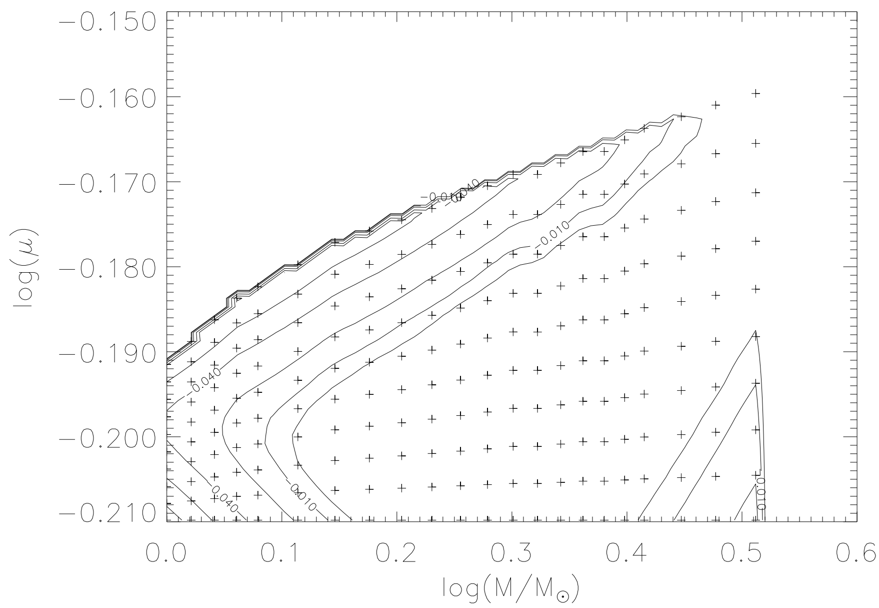

Figure 4.6: The difference in $\log L/\mathrm{L}_\odot$ between the computed artificial models (CAM) and the fit to the $L-M-\bar{\mu}$-surface. Contourlevels are shown for $\log(L_{\mathrm{CAM}}/\mathrm{L}_\odot) - \log(\mathrm{L}_{\mathrm{fit}}/\mathrm{L}_\odot)$ = -0.2,-0.1,-0.08,-0.06,-0.04,-0.02,-0.01 and -0.005.

4.3 Comparison of Simplified and Evolutionary Models

To check if the simplified models really fit to detailed evolutionary models, I will compare them in this section with single star evolutionary models and binary evolutionary models, for different masses.

4.3.1 Single Star Evolutionary Models

Figure 4.7 and compare single star evolutionary models of stars with resp. $1.6\mathrm{M}_\odot, 2.3\mathrm{M}_\odot$ and $3.0\mathrm{M}_\odot$ with the simplified numerical models and the $L - M - \bar{\mu}$-relation of Eq. 4.17. As can be seen in this figure, the numerical models

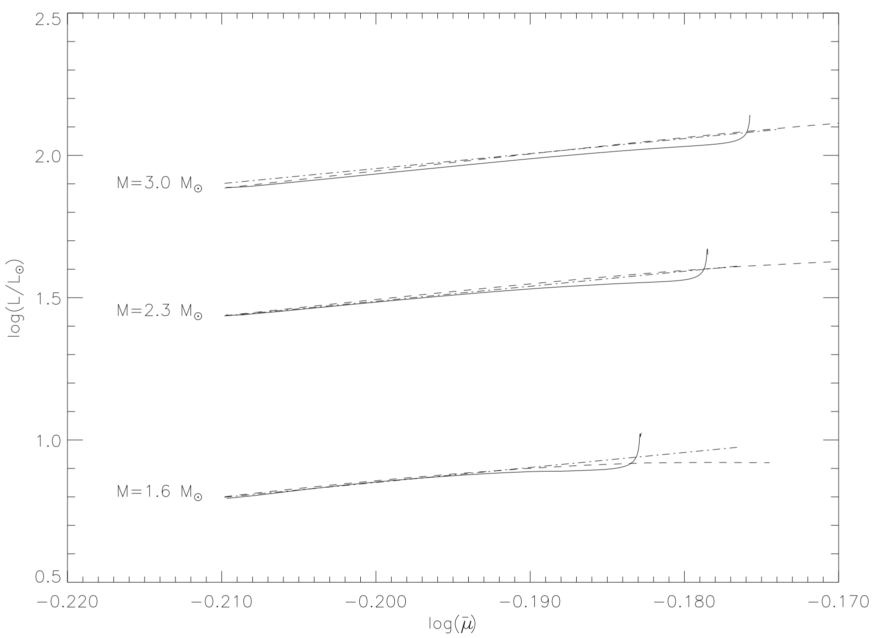

Figure 4.7: Comparison of detailed single star evolutionary models (solid line) with the simplified numerical models (dashed line) and the $L - M - \bar{\mu}$-relation of Eq. 4.17 (dash-dotted line) in the $\log L - \log \bar{\mu}$-plane. This figure shows sequences for stars of $1.6\mathrm{M}_\odot, 2.3\mathrm{M}_\odot$ and $3.0\mathrm{M}_\odot$. All models start at $\log(\bar{\mu}) = -0.210$ with a homogeneous composition of $X = 0.70, Y = 0.28, Z = 0.02$. The detailed single star model of $1.6\mathrm{M}_\odot$ reach the end of core hydrogen burning phase at $\log \bar{\mu} = -0.183$ ($\bar{\mu} = 0.656$). The detailed evolutionary model for the $2.3\mathrm{M}_\odot$-star reaches the end of the main sequence at $\log \bar{\mu} = -0.1785$ ($\bar{\mu} = 0.663$) and for the $3.0\mathrm{M}_\odot$-star at $\log \bar{\mu} = -0.1785$ ($\bar{\mu} = 0.663$). Both the simplified numerical models (dashed lines) and the fit to the models (dash-dotted lines) are too luminous by a few percents but never more than 12%.

reproduce quite well the detailed stellar models during the main sequence phase. The deviation in luminosity for all curves is rougly less then 5%, but always less then 12%. The line representing simplified models (dash-dotted) exceeds the $\bar{\mu}$-value at the terminal age main sequence, because the part of the star where the abundances equals the central abundances is larger than the convective core in detailed models. The little downturn of the numerical models at $\bar{\mu}$-values for the end of the main sequence seems to be comparbable to a similar downturn in the detailed models, but is not completely understood. The line corresponding to Eq. 4.17 does not show this feature, since this relation is exponential in the mass and the average mean molecular weight, and thus must be a straight line in the $\log L - \log \bar{\mu}$-diagram.
The conclusion from these figures can be, that the $L-M-\bar{\mu}$-relation of Eq. 4.17 is a good approximation within the mass range 1.6M$_\odot$–3.0M$_\odot$, and presumably beyond.

4.3.2 Binary Evolutionary Models

To compare the $L-M-\bar{\mu}$-relation of Eq. 4.17 with detailed binary evolution we calculated three different binary evolutionary models. The first (Fig. 4.8, upper panel) started with a black hole of 5.8 M$_\odot$, a donor star of 3.5 M$_\odot$ and with a period of 1.31d (in short: $5.8+3.5-1.31$), the second (Fig. 4.8, lower panel) and third (Fig. 4.9) $4.35 + 2.5 - 0.98$ and $4.8 + 4.5 - 0.93$ respectively. Comparing the $L - M - \bar{\mu}$-relation of Eq. 4.17 with detailed binary evolution models in Fig. 4.8 and Fig. 4.9 (upper panel), we can see that the fit is in good agreement with the binary evolutionary models, with a deviation in the luminosity of less then 12%, except for the model of 4.5M$_\odot$ at the end of the main sequence where the deviation is roughly 25%. All fits start overluminous, a similar feature as observed for fits of single star models, but during the mass transfer phase this is corrected, and at the end of the main sequence phase the fit is at the same level as the luminosity of detailed models or slightly underluminous.
Figure 4.9 (lower panel) shows the effect of mass loss on the chemical profile of the star, and shows that the actual convective core is much smaller then the initial core. The initial convective core ($M_{\rm core,initial} \approx 1.05M_\odot$) had a mass that is now about 60% of the whole star ($M_{\rm tot} = 1.8$M$_\odot$), the star thus lost about 2.7M$_\odot$ of its envelope.

From these figures it is clear that the $L - M - \bar{\mu}$-relation of Eq. 4.17 is also valid for stars which lose mass during their main sequence phase, irrespective of when the mass transfer phase starts, how much mass is lost, or which mass the star initially has. The highest value of the average mean molecular weight that has been reached by the binary models is $\log \bar{\mu} = -0.13$. Only stars that loose a significant amount of mass reach this value. From the comparison of detailed evolutionary models with the $L - M - \bar{\mu}$-relation we can conclude that this relation is useful until this value, and possibly also beyond.

4.4 Conclusion

In this chapter we first investigated mass luminosity relations derived from homology relations. These relations give an expression for the luminosity in terms of the mass and the mean molecular weight, but were only suitable for chemically homogeneous stars. As this is hardly ever the case, we could not apply these relations for fitting our detailed stellar models.
In order to obtain an accurate measure for the chemical composition, we introduced the average mean molecular weight, as the sum of the local mean molecular weight averaged over the mass. With this new quantity we were able to calculate a relation between the mass, the luminosity and the average mean molecular weight, by using artificially constructed stellar models.
We compared this relation with detailed single star evolutionary models and with detailed binary evolutionary models. It turned out that single star models are well represented by this relation, except the short time before the terminal-age main sequence, when detailed evolutionary models are out of equilibrium. The mass range in which this relation is tested is from $1.6 - 3.0 \mathrm{M}_{\odot}$, but it is expected that also for higher masses this relation is useful. For lower masses there is some deviating behaviour caused by the development of an outer convection zone (Kippenhahn & Weigert, 1990, Page 208) which decreases the radius.
Comparison with binary evolutionary models reveals that the Mass-Luminosity-Average mean molecular weight relation represents the models within the range of $-0.210 < \log \bar{\mu} \lesssim -0.13$ with errors less than 12%. There were no models to compare this relation for values of $\log \bar{\mu} > -0.13$, but it is not inconceivable that this relation is useful to higher values of $\log \bar{\mu}$. The lower mass limit for which the relation is useful, is approximately $1.30 \mathrm{M}_{\odot}$, because of the development of the convective envelope which decreases the radius and therefore changes the luminosity.
Overall we can conclude that the calculated mass-luminosity-average mean molecular weight relation is applicable to stars both with and without mass loss.

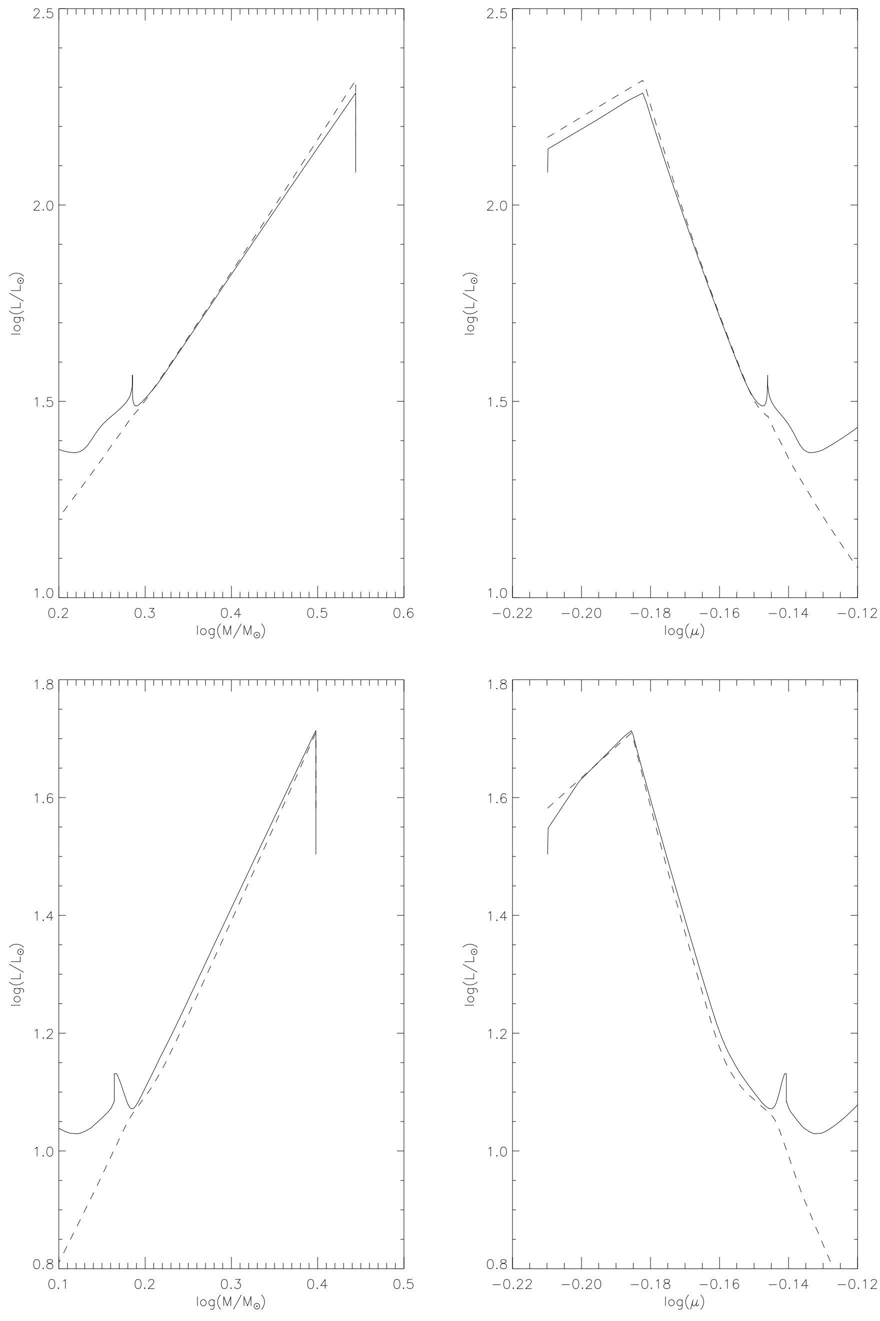

Figure 4.8: The evolutionary model (solid lines) of a $3.5\mathrm{M}_\odot$-star (upper panel) and a $2.5\mathrm{M}_\odot$-star (lower panel) in a binary, that starts mass tranfer during the main sequence phase, compared to the empirical relation of Eq. 4.17 (dashed line). The mass transfer phase for the $3.5\mathrm{M}_\odot$-star starts at $\log(\bar{\mu}) \approx -0.18$ as is most clearly from the upper right panel. The end of the main sequence (indicated by a sudden increase in lumininosity) is reached at a mass of $1.95\mathrm{M}_\odot, (\log(\mathrm{M}/\mathrm{M}_\odot) = 0.29)$ and at $\bar{\mu} = 0.716$), $(\log(\bar{\mu}) = -0.145)$. For the $2.5\mathrm{M}_\odot$-star the mass transfer phase starts at $\log(\bar{\mu}) \approx -0.185$ and the end of the main sequence is reached at a mass of $1.48\mathrm{M}_\odot, (\log(\mathrm{M}/\mathrm{M}_\odot) = 0.17)$ and at $\bar{\mu} = 0.724$), $(\log(\bar{\mu}) = -0.145)$

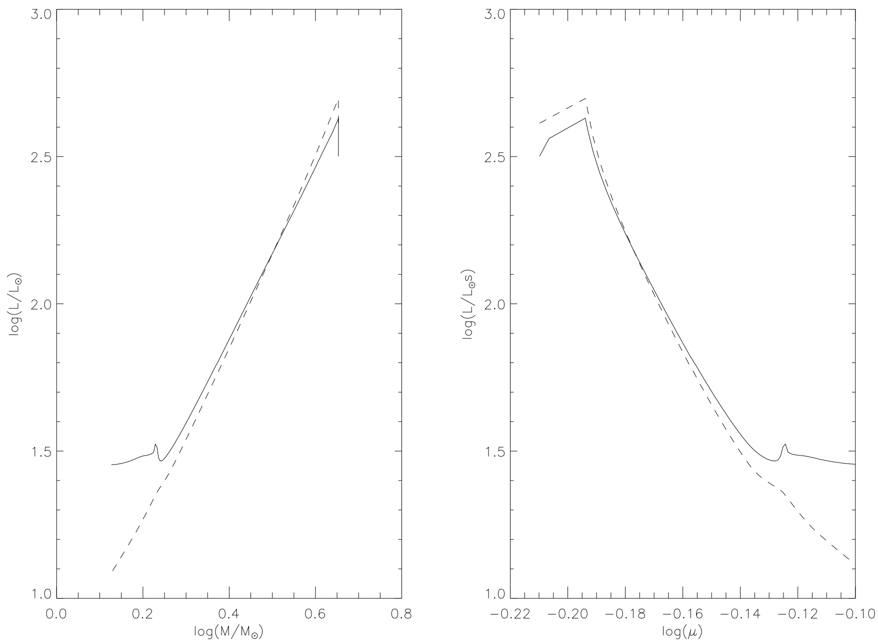

Figure 4.9: Same figure as Fig. 4.8, but for a star with a mass of $4.5\mathrm{M}_\odot$ which starts mass transfer at $\bar{\mu} = -0.195$ and reaches the end of the main sequence at $\bar{\mu} = -0.125$ and a mass of $1.78\mathrm{M}_\odot$.

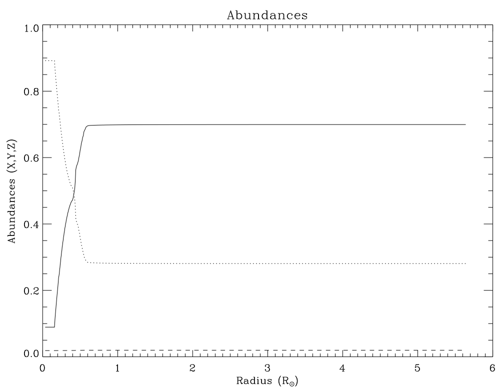

Figure 4.10: The hydrogen, helium and metal profiles at the end of the main sequence ($M = 1.78\mathrm{M}_\odot$) for the star which is discussed in the upper panel. The solid line shows the hydrogen abundance as a function of the radius (lower left) and of the mass (lower right), the helium abundance is showed with a dotted line, and the metals with a dashed line. The mass loss phase started at a helium abundance of $Y = 0.5$, when the convective core had a mass of about $0.8\mathrm{M}_\odot$.

Chapter 5

Reconstructing evolved Main-Sequence Stars

In the previous chapter the conclusion was drawn, that the derived $L - M - \bar{\mu}$-relation could be used for main sequence stars without mass loss as well as for main sequence stars with mass loss, for values between $\log \bar{\mu} \approx -0.21$ and -0.13. Using this result I develop in this chapter a method with which I am able to construct a stellar model that displays all the observed properties of a certain observed main sequence star. Important in this method, which will be discussed in Section 5.1, will be the mass which determines the luminosity, and the shape of the chemical profile which determines the radius and the temperature. In Section 5.2 the secondary of GRO J1655-40 as observed by Orosz & Bailyn (1997) will be reconstructed, while in Section 5.3 the secondary as observed by Beer & Podsiadlowski (2002) will be reconstructed. In section 5.4 the conclusions will be drawn for this part of the work.

5.1 The Method

For a given luminosity L and mass M of a star we are able to derive with Eq. 4.17 the average mean molecular weight $\bar{\mu}$ inside the star. We assume that the composition profile of the star is a stepfunction, with the 'step' at the core-envelope boundary. The composition is determined by the hydrogen abundance, which is given by

$$X(M_{\rm r}) = \begin{cases} X_{\rm c} & M_{\rm r} < M_{\rm core} \\ X_{\rm env} & M_{\rm r} > M_{\rm core} \end{cases} \tag{5.1}$$

with X the hydrogen abundance as a function of the radial mass coordinate, $X_{\rm c}$ the hydrogen abundance in the core, $X_{\rm env}$ the hydrogen abundance in the envelope and $M_{\rm core}$ the mass of the core. Furthermore, assuming $Z = 0.02$ and $Y = 1 - Z - X$ (at the surface $X = 0.70, Y = 0.28, Z = 0.02$) we can define the average mean molecular weight as

$$\begin{aligned}\frac{M_{\rm tot}}{\bar{\mu}} &= \frac{M_{\rm core}}{\mu_{\rm c}} + \frac{M_{\rm env}}{\mu_{\rm env}}, \qquad (5.2)\\ \text{with } \mu_{\rm env} &= (2X_{\rm env} + 0.75Y_{\rm env} + 0.5Z_{\rm env})^{-1} = 0.617\\ \text{and } \mu_{\rm c} &= (2X_{\rm c} + 0.75Y_{\rm c} + 0.5Z_{\rm c})^{-1} = (1.25X_{\rm c} + 0.736)^{-1}\,.\end{aligned}$$

These two relations and $M_{\rm env} = M_{\rm tot} - M_{\rm core}$ define a unique function in which the core mass is only dependent on $X_{\rm core}$

$$(\bar{\mu}^{-1} - \mu_{\rm env}^{-1})M_{\rm tot} = (\mu_{\rm c}^{-1} - \mu_{\rm env}^{-1})M_{\rm core}. \qquad (5.3)$$

This gives finally

$$M_{\rm core} = M_{\rm tot}\left(\frac{\bar{\mu}^{-1} - \mu_{\rm env}^{-1}}{\mu_{\rm c}^{-1} - \mu_{\rm env}^{-1}}\right). \qquad (5.4)$$

With these values for $M_{\rm tot}$, $M_{\rm core}$ and $X_{\rm core}$ we are able to construct a stellar model.
When we keep the total mass and $\bar{\mu}$ fixed, we have the freedom to vary the chemical composition in the core to construct models with different core masses. Figure 5.1 shows several possible stellar models (for a fixed mass of $2.3{\rm M}_\odot$ and fixed $\bar{mu}$) with different core masses and core hydrogen abundances. For stars with a low core hydrogen abundance the core is small, compared to the total mass. That means that these stars did not lose a huge amount of mass during their evolution. On the contrary, stars with a high hydrogen abundance in their core, have a large core compared to their total mass, and thus must have lost a huge amount of matter during their evolution.

Calculating different stellar models with different core masses and core abundances, gives models with roughly a constant luminosity as expected from Eq. 4.17, but with different radii and temperatures (see Table 5.1).
As can be seen, the convective core after relaxation is smaller than the calculated core mass for each model, due to the steep chemical discontinuity. Besides this effect, the steep chemical discontinuity also gives rise to a lower temperature and a larger radius, than one would expect for actual stars with the same mass and average mean molecular weight. Decreasing the slope of this discontinuity gives stellar models that fit better to reality. Again, changing the slope does not affect the luminosity of the stellar model, but only changes the temperature and the radius. Although the slope of the chemical profile in reality will not exact be a linear function of the relative mass coordinate, here we model it with a linear function for simplicity.

Most of the calculated models will not fit to the observations, because their temperature is far outside the errorbar. Therefore only the models that are inside the errorbars or in the close vicinity are selected to be calculated again with a smoother chemical transition between the core and the envelope.
Calculating again different models with different slopes in their chemical profiles (see Fig. 5.2), gives models (constant in luminosity) with a minimum core

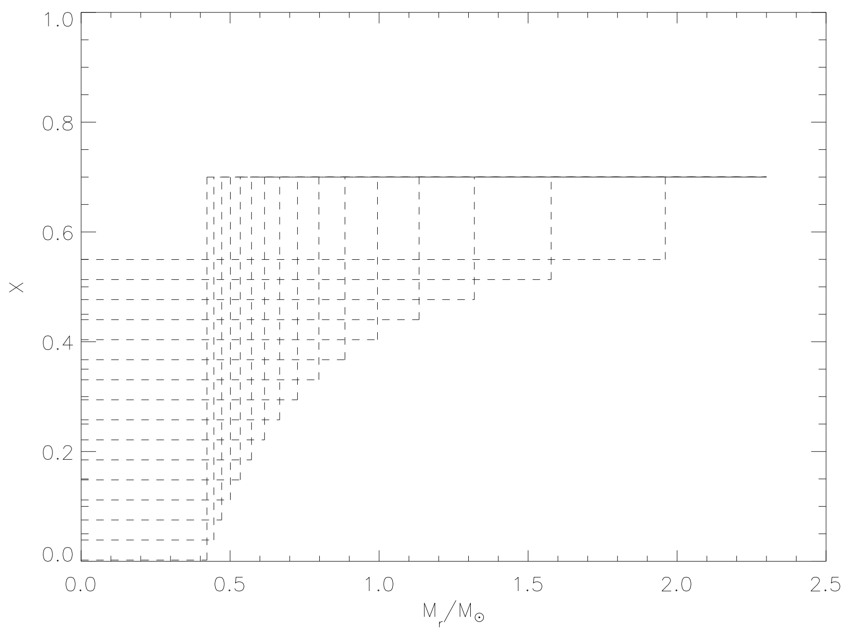

Figure 5.1: Different hydrogen profiles for various values of X and $M_{\rm core}$. The total mass of the star is taken as $2.3\mathrm{M}_{\odot}$, the average mean molecular weight ($\bar{\mu} = 0.685$) and the surface abundances are $X = 0.70, Y = 0.28, Z = 0.02$. For larger values of the Hydrogen abundance the core must be bigger in order to reach the right value of the mean- mean molecular weight. The properties of the models are shown in Table 5.1.

mass (where the hydrogen abundance starts to increase) and a maximum core mass (where the hydrogen abundance reaches the level of the surface hydrogen abundance) and with different temperatures and radii. When we compare these temperatures and radii with the observed values, the models that are within the errorbars of the observation, give a minimum and a maximum core mass. If the stellar model has a convective core (which is the case for stars with masses roughly above $1.5\mathrm{M}_{\odot}$), the minimum core-mass and the convective core should be of equal mass, because the convective core shrinks during its evolution giving rise to a constant hydrogen abundance in the core but a increasing abundance outside.
The maximum core mass is directly related to the initial ZAMS mass of the star, from which, together with the actual mass, the mass loss during the evolution can be derived.

Table 5.1: Properties of stellar models with different core masses and core hydrogen abundances after relaxation. All stars have the same mass of 2.3$M_\odot$ and the same average mean molecular weight ($\bar{\mu} = 0.685$). The chemical profiles are displayed in Fig 5.1. The first column contains the total mass, the second column contains the mass of the core, as derived from Eq. 5.4, the third column is the mass of the convective core after relaxation, the fourth is the surface luminosity of the relaxed star, the fifth is the surface temperature, the sixth is the radius of the star and the last column contains the core hydrogen abundance. Models with a hydrogen abundance higher than 0.58 have cores that are larger than the whole star, and are thus unphysical.

$M_{\rm tot}/{\rm M}_\odot$	$M_{\rm core}/{\rm M}_\odot$	$M_{\rm cc}/{\rm M}_\odot$	$L/{\rm L}_\odot$	T/K	$R/{\rm R}_\odot$	$X_{\rm H,core}$
2.30	1.96	0.46	1.72	10726	2.13	0.5497
2.30	1.58	0.44	1.74	10243	2.37	0.5132
2.30	1.32	0.42	1.74	9881	2.56	0.4767
2.30	1.13	0.41	1.74	9568	2.73	0.4402
2.30	0.99	0.38	1.74	9284	2.89	0.4037
2.30	0.89	0.36	1.73	9025	3.05	0.3672
2.30	0.80	0.34	1.73	8774	3.22	0.3307
2.30	0.73	0.32	1.72	8530	3.38	0.2942
2.30	0.67	0.30	1.71	8288	3.55	0.2577
2.30	0.62	0.27	1.71	8042	3.74	0.2212
2.30	0.57	0.26	1.70	7807	3.91	0.1847
2.30	0.53	0.24	1.69	7555	4.12	0.1482
2.30	0.50	0.21	1.68	7314	4.32	0.1117
2.30	0.47	0.20	1.67	7033	4.62	0.0752
2.30	0.45	0.18	1.65	6773	4.91	0.0387
2.30	0.42	0.16	1.65	6628	5.10	0.0022

5.2 Application I - to Orosz & Bailyn

In this section I will, following the method described above, reconstruct a main sequence star that displays the properties of the star observed by Orosz & Bailyn (1997). In Section 5.2.1 the fine tuning of the average mean molecular weight is done, in Section 5.2.2 the fine tuning in the mass and finally in Section 5.2.3 the finetuning of the chemical profile is done.
In addition to Section 3.1 the properties of the secondary are summarized here. Orosz & Bailyn (1997) found for the mass of the black hole $M_1 = 7.02 \pm 0.22{\rm M}_\odot$, for the secondary $M_2 = 2.34 \pm 0.12{\rm M}_\odot$, the temparature of the secondary $T_{\rm eff} = 6500 \pm 250K$, the luminosity $L = 46.6 \pm 13.6{\rm L}_\odot$ and the radius $R = 4.85 \pm 0.08{\rm R}_\odot$. Because the errorbars on the radius are much tighter than on the luminosity, the Radius-Temperature plane is used to plot the models.

5.2.1 Fitting the Average Mean Molecular Weight

Using the inferred mass and luminosity (Orosz & Bailyn, 1997) we can derive with Eq. 4.17 the average mean molecular weight to be of the order of $\bar{\mu} = 0.675$,

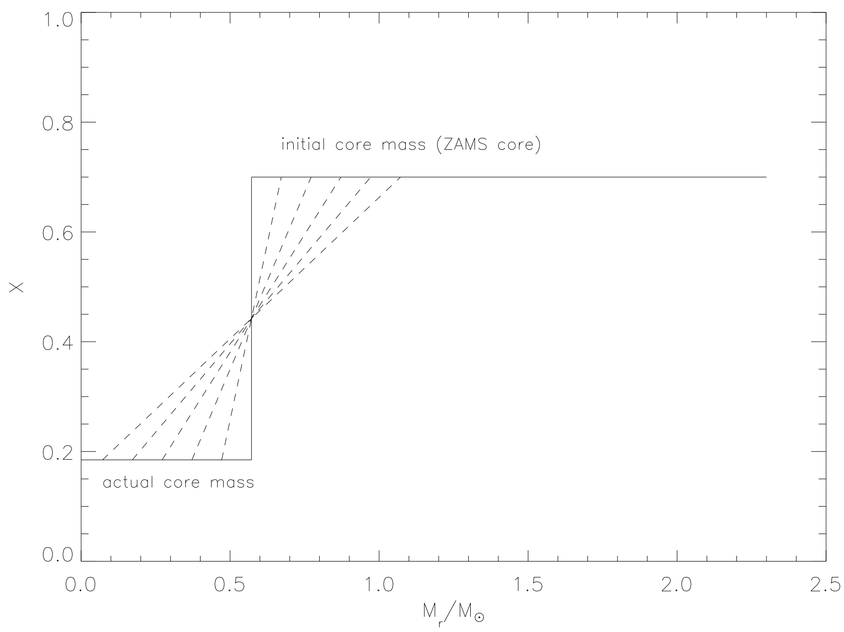

Figure 5.2: Example of models with constant average mean molecular weight but different chemical profiles, for the same star as in Figure 5.1. The initial core mass and the actual core mass are also indicated.

which is above the value for ZAMS stars $\bar{\mu} = 0.617$ ($X = 0.70, Y = 0.28, Z = 0.02$) and also slightly above the value for terminal age main sequence stars of $2.34\mathrm{M}_\odot$ (which is in detailed evolutionary models about $\bar{\mu} = 0.668$). That means that the star must have had mass transfer during its main sequence evolution in order to reach this value of the mean molecular weight. In Figure 5.3 models for different values of the average mean molecular weight and the core hydrogen abundance are shown. It clearly shows that a $2.30\mathrm{M}_\odot$ star with $\bar{\mu} = 0.668$ could not display the properties of the secondary in GRO J1655-40. Increasing the average mean molecular weight causes a decrease of the temperature and an increase of the radius, which brings the model closer to the observed point. However, none of the models shown in Figure 5.3 could reproduce the observed properties (i.e. radius and temperature) of the secondary, all of them are too hot and/or too big, and as we will we see in section 5.2.3 changing the chemical profile can not alter this enough.

5.2.2 Fitting the Mass

As concluded in the previous section, the models with a mass of $M_{\mathrm{tot}} = 2.30\mathrm{M}_\odot$ can not reproduce the observed properties of the system. Therefore in this

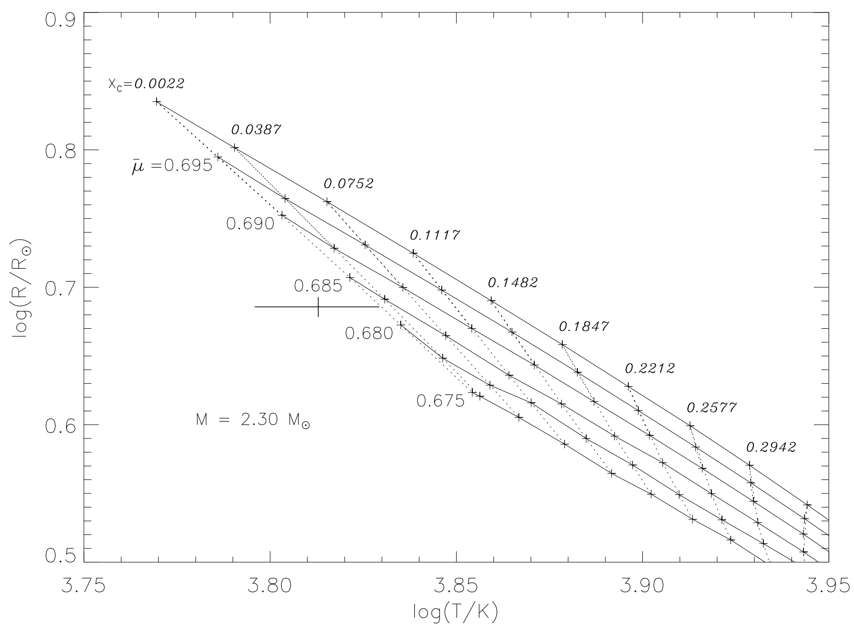

Figure 5.3: For several values of the average mean molecular weight a sequence of models with a increasing core hydrogen abundance is calculated and plotted in the radius-temperature plane. The stellar models all have a mass of $2.30\mathrm{M}_\odot$ and are relaxed into thermal and hydrostatic equilibrium. All models with the same average mean molecular weight ($0.675 \ldots 0.700$) are connected with a full line, all models with the same core hydrogen abundance (values in italic) are connected with a dotted line. The point with errorbars is the observed point of Orosz & Bailyn (1997).

section the effect of changing the mass is investigated. Calculating models with the same value for $\bar{\mu}$ but a lower mass (and thus a slightly lower luminosity) give results that are more in agreement with the value of Orosz & Bailyn (1997). From Figure 5.4 we can conclude that the model with $M_{\mathrm{tot}} = 2.20\mathrm{M}_\odot$ and a hydrogen abundance of $X_{\mathrm{core}} = 0.04$ fits best to the observations. Problematic in this case, however, is the fact that the core hydrogen abundance is extremely low ($X < 0.04$). The only way to correct for this is to increase the average mean molecular weight as can be seen from Figure 5.3. What happens is that increasing the $\bar{\mu}$ and choosing a higher core hydrogen abundance implies a larger core (see Eq. 5.4). By the way, this means that the star must have had an episode of mass loss, because the core then is too large compared to the whole star.

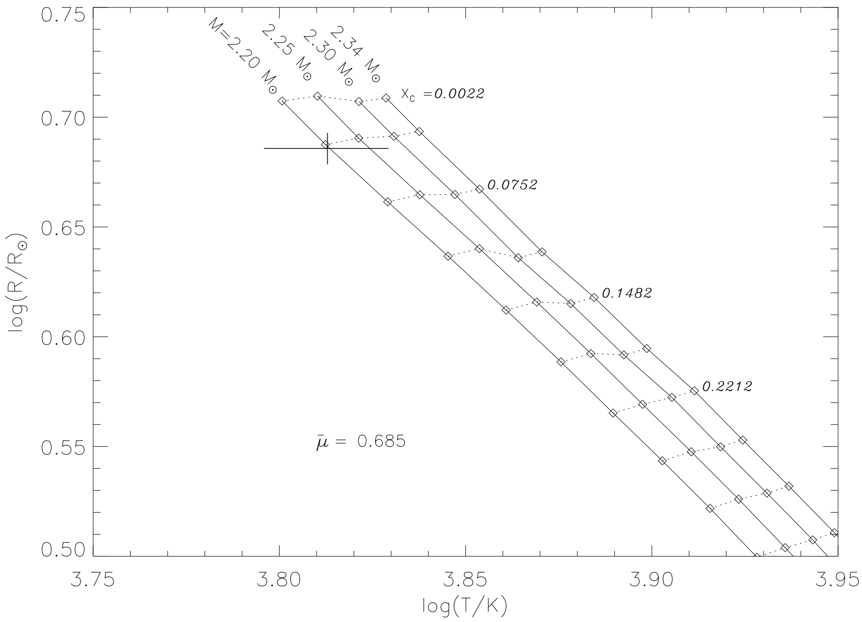

Figure 5.4: Four sequences with each different mass ($M = 2.20, 2.25, 2.30\&2.34\mathrm{M}_{\odot}$) and increasing hydrogen abundance in the core, are plotted in the radius-temperature plane. All models with the same mass are connected with a full line, all models with the same core hydrogen abundance (values in italic) are connected with a dotted line. The point with errorbars is the observed point of Orosz & Bailyn (1997).

5.2.3 Fitting the Chemical Profile

The effect of changing the chemical profile is shown in Figure 5.5. Starting at a core hydrogen abundance of $X = 0.0022$ (for the model with $M_{\mathrm{tot}} = 2.20\mathrm{M}_{\odot}$) and decreasing the slope of the chemical profile (see Fig. 5.2) decreases the radius of the star and increases the temperature of the star. The model which has a slope of $\Delta X/\Delta M = 2.61$, which means that the transition zone in which the hydrogen abundance increases from the value in the core to the value at the surface has a mass of $0.27\mathrm{M}_{\odot}$, fits best to the observed properties. The mass of the minimum core is about $0.26\mathrm{M}_{\odot}$ which should be equal to the convective core of the model, which is with $0.15\mathrm{M}_{\odot}$ a bit smaller than expected. The mass of the maximum core is about $0.53\mathrm{M}_{\odot}$ and is per definition the size of the initial ZAMS core. From ZAMS models we can conclude that a star with a mass slightly below $2.8\mathrm{M}_{\odot}$ initially has a convective core of $0.53\mathrm{M}_{\odot}$. The model, of the sequence with a mass of $M_{\mathrm{tot}} = 2.25\mathrm{M}_{\odot}$ that is within the errorbars, has a temperature that is a bit too high. It has a slope of 2.57 which means that the transition region has also a mass of $0.27\mathrm{M}_{\odot}$. The mass of the minimum

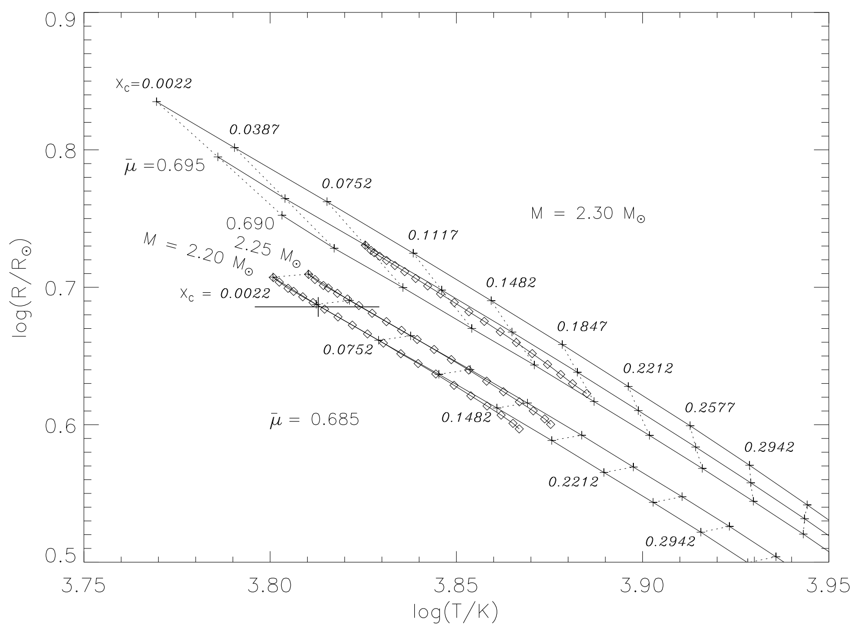

Figure 5.5: This figure shows partially the contents of Fig. 5.3 (change in $\bar{\mu}$ uppermost three solid lines, for $M_{\rm tot}$ = 2.30M$_\odot$) and Fig. 5.4 (change in mass (2.20M$_\odot$ and2.25M$_\odot$), lowermost two lines, for $\bar{\mu} = 0.685$) and overplotted three sequences of models with changing slope. The two sequences with masses 2.20M$_\odot$ and 2.25M$_\odot$ are starting at $X = 0.0022$, and with mass 2.30M$_\odot$ is starting at $X = 0.0752$. The point with errorbars indicates the observed radius and temperature by Orosz & Bailyn (1997).

core is 0.27M$_\odot$, and compared to the actual convective core, which has a mass of 0.16M$_\odot$, this is too large. The mass of the maximum core is 0.54M$_\odot$ which corresponds to a initial ZAMS mass of 2.8M$_\odot$.

5.2.4 Discussion

The numerical models that are derived are in the previous are always compared with the observed point in the temperature-radius plane, since the errorbars in the radius are much smaller than the errorbars in the luminosity. If we, however, compare the derived models with the errorbars in the luminosity-temperature plane, there are much more models that fit to the observations, as is shown in Figure 5.6. The time fails to digest deep into this plot, but it is clear that models with a mass of 2.30M$_\odot$ are within the errorbars and that the core hydrogen abundance will be $0.02 < X_{\rm c} < 0.07$. The calculations show that these models should have had initially masses of $2.8 < X_{\rm c} < 3.5$.

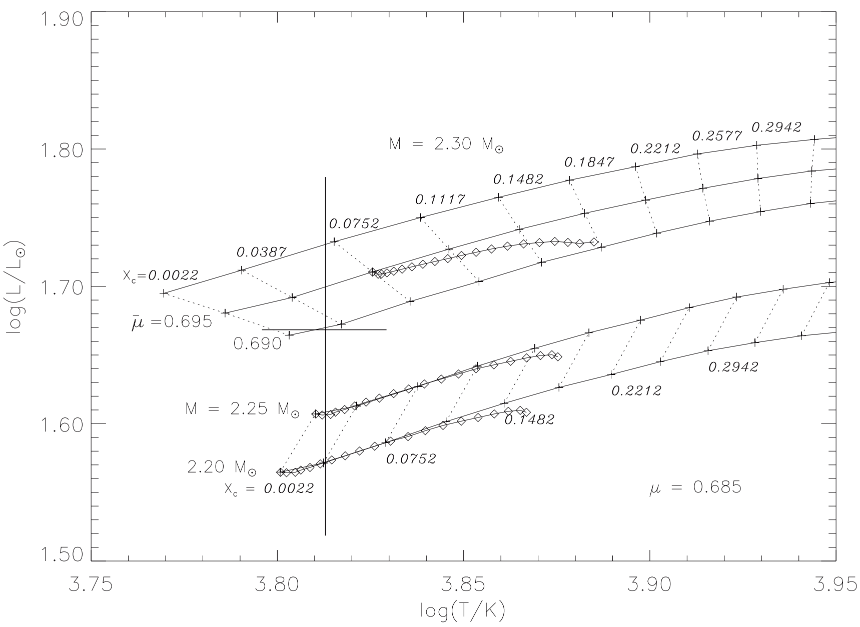

Figure 5.6: The same figure as Fig. 5.5 but instead of the radius at the y-axis now the luminosity is plotted. When one compares this Figure and Fig. 5.5 with each other, the conclusions is that there are much more models that fit into the errorbars.

5.2.5 Summary

The secondary as observed by Orosz & Bailyn is best reproduced with a stellar model that has a mass between 2.20 $M_\odot$ and 2.25 $M_\odot$ and that has an average mean molecular weight of $\bar{\mu} = 0.685$ with a central hydrogen abundance $0.02 < X_c 0.05$. This gives stellar models with temperatures $6480 < T_{\rm eff}/K < 6760$, luminosity $1.57 < L/L_\odot < 1.62$ and radii $4.77 < R/R_\odot < 4.93$. The initial zero-age main sequence star should have had a mass of $2.8 < M_i/M_\odot < 2.9$. If we take the larger errorbars on the luminosity into account this range will be widened to $2.8 < M_i/M_\odot < 3.5$.

5.3 Application II - the point of Beer & Podsiadlowski

As discussed in Section 3.1 in a recent paper Beer & Podsiadlowski (2002) claimed to have derived a significantly lower mass for the black hole and its companion in GRO J1655-40. As this mass is the lowest claimed value for the secondary I will construct a stellar model for this mass too that will display the observed properties. In Section 5.3.1 the mass will be investigated, in Section 5.3.2 the average mean molecular weight will be fine tuned, and the chemical profile will be optimized in Section 5.3.3.
In addition to Section 3.1 the observed properties of the secondary (according to Beer & Podsiadlowski, 2002) are summarized here. Beer & Podsiadlowski (2002) derived a mass of the secondary corresponding to $1.45 \pm 0.35 M_\odot$ with a luminosity of $L = 21.0 \pm 6.0 L_\odot$ and a temperuature of $T_{\rm eff} = 6150 \pm 350$K and a black hole mass of $5.4 \pm 0.3 M_\odot$. From the fact that Beer & Podsiadlowski (2002) did not give a value for the radius (allthough it could be derived easily from the relation between the radius, luminosity and temperature or, using the fact that the system is a Roche lobe filling system, from the Roche lobe radius, Eq. 2.3), the Luminosity-Temperature plane is used to plot the models.

5.3.1 Fitting the Mass

With use of the mass-luminosity-average mean molecular weight relation (Eq. 4.17) and the derived mass of Beer & Podsiadlowski (2002) we can calculate the average mean molecular weight needed to reproduce the observed Luminosity. We derived for a $1.3 M_\odot$ star an average mean molecular weight of $\bar{\mu} = 0.910$[1] and for a $1.45 M_\odot$ star $\bar{\mu} = 0.837$. These values for the average mean molecular weight are far above the values that stars of these masses should have at the end of the main sequence ($\bar{\mu} \sim 0.65$), but also give a luminosity that is much too high compared with the observed point (see Fig. 5.8 and Fig. 5.9). In Figure 5.7 two sequences of models with different masses and with a more suitable value for the average mean molecular weight are shown. These sequences both have

[1]Note that this value for the average mean molecular weight is far beyond the limiting value derived in Section 4.3.2.

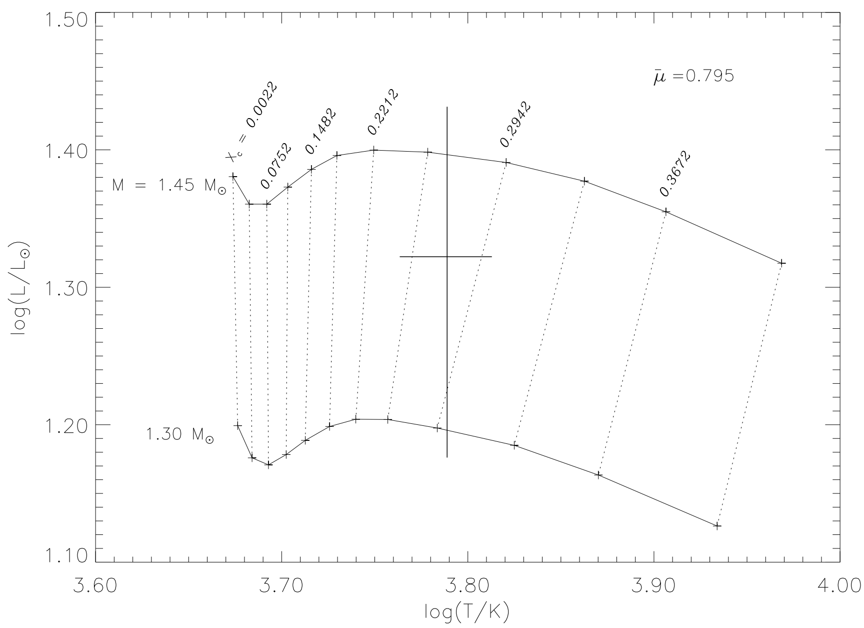

Figure 5.7: Same as Fig. 5.4, but now for a stars with masses of 1.30 and 1.45M$_\odot$, and plotted in the luminosity-temperature plane. Both sequences are calculated with a average mean molecular weight of $\bar{\mu} = 0.795$. The point with errorbars is the observed point of Beer & Podsiadlowski (2002).

models that are within the errorbars of the observed point.
From this figure we can *not* conclude that the observed point can only be reproduced with a model that has a mass between 1.30M$_\odot$ and 1.45M$_\odot$, because for a lower average mean molecular weight it is possible to create a model with a higher mass that could be within the errorbars of luminosity and temperature. It is however clear that the hydrogen abundance in the core must be approximately 0.25, which means that the transition between the core and the envelope, using Eq. 5.4, is approximately at $0.63 \times M_{\rm tot}$, which implies a significant mass loss in the past.

5.3.2 Fitting the Average Mean Molecular Weight

Some models with different values for the average mean molecular weight have been calculated in order to obtain an appropriate range in $\bar{\mu}$ that gives models within the errorbars of the observed point. For models with $M = 1.30$M$_\odot$ the lowest value for the average mean molecular weight, that is within the errorbars, is $\bar{\mu} = 0.795$ as can be seen from Figure 5.8. Allthough the maximum value for a star of 1.30M$_\odot$ is not so clear from the figure it will be approximately $\bar{\mu} = 0.855$.

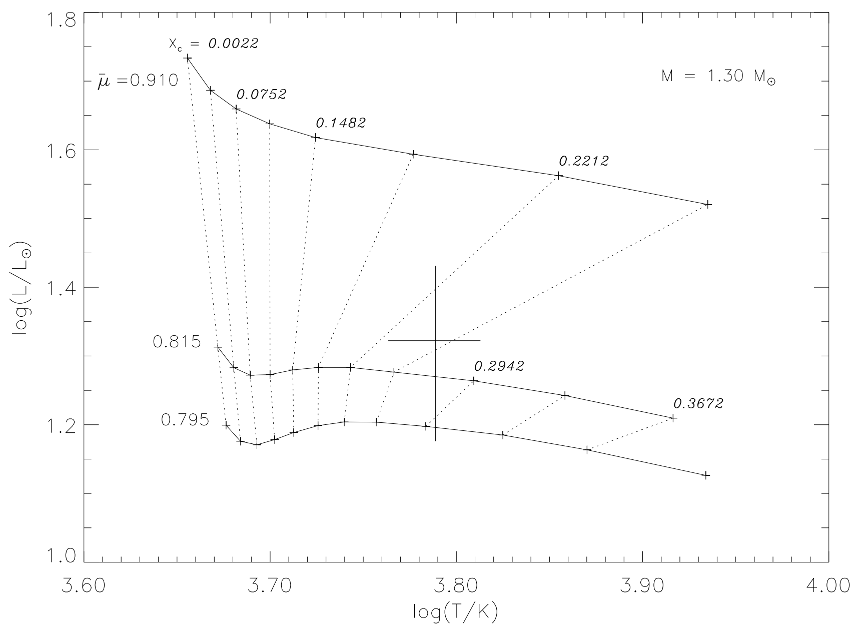

Figure 5.8: Same as Fig. 5.3, but for models with a mass of $M = 1.30\mathrm{M}_\odot$. Sequences are calculated for $\bar{\mu} = 0.795, 0.815$ and 0.910. On the left axis now the luminosity is plotted instead of the radius. The point with errorbars is the observed point of Beer & Podsiadlowski (2002).

For these models the hydrogen abundance in the core will be between $X_\mathrm{c} = 0.20$ and $X_\mathrm{c} = 0.30$. The core mass is between $0.85\mathrm{M}_\odot$ and $0.93\mathrm{M}_\odot$.

For a star of $1.45\mathrm{M}_\odot$, similar to a $1.30\mathrm{M}_\odot$ star, also stellar models with different values for the average mean molecular weight have been calculated. The results are plotted in Figure 5.9. The limiting values for the average mean molecular weight for this mass are approximately $\bar{\mu} = 0.755$ for the minimum luminosity and $\bar{\mu} = 0.795$ for the maximum luminosity. The core hydrogen abundance is again between $X_\mathrm{c} = 0.20$ and $X_\mathrm{c} = 0.30$. The core mass is between $0.82\mathrm{M}_\odot$ and $0.88\mathrm{M}_\odot$.
From these calculations we can once again conclude that the stars should have lost a significant amount of mass, because their core mass is too large compared to their total mass.

5.3.3 Fitting the Chemical Profile

To create a model that is more in agreement with a detailed stellar model (and hopefully the reality) we have to change the discontinuous chemical transition into a smooth transition. The $1.30\mathrm{M}_\odot$ models with an average mean

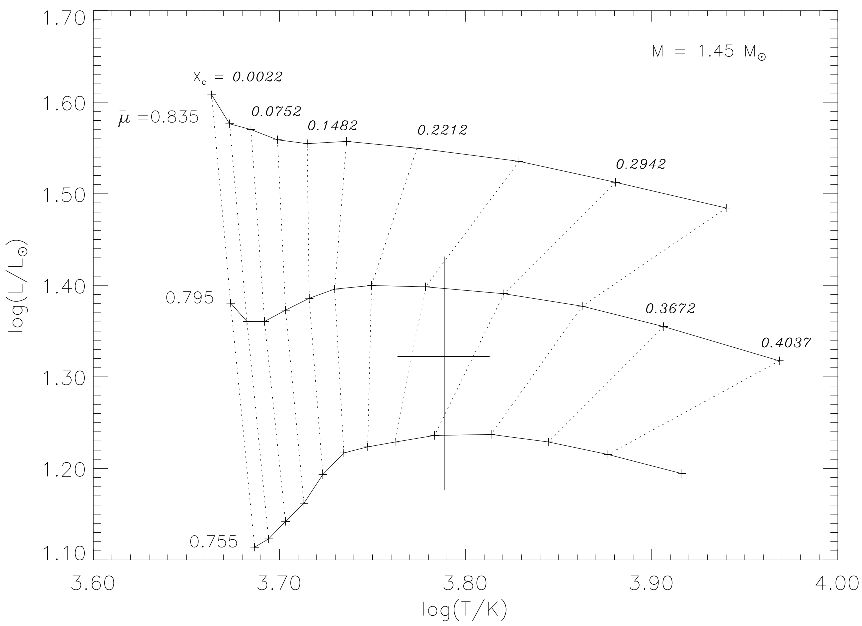

Figure 5.9: Same as Fig 5.8 but for models with a mass of 1.45M$_\odot$. Sequences are calculated for $\bar{\mu} = 0.755, 0.795$ and 0.835.The point with errorbars is the observed point of Beer & Podsiadlowski (2002).

molecular weight of $\bar{\mu} = 0.815$ and a central hydrogen abundance of $X_c = 0.2212$ and 0.2577 are here considered. The effect of the flattening the slope of the hydrogen profile in the transition region is shown in Fig. 5.10. As can be seen, all models with a central hydrogen abundance of $X_c = 0.2522$ are within the errorbars what means that the size of the transition region could vary between 0M$_\odot$ and 0.69M$_\odot$, giving a original convective core mass at ZAMS between 0.92M$_\odot$ and 1.24M$_\odot$. These masses for the original cores implies ZAMS masses between 4.1M$_\odot$ and 5.1M$_\odot$.
The 1.30M$_\odot$ model with a core hydrogen abundance of $X_c = 0.2212$ at an average mean molecular weight of $\bar{\mu} = 0.815$ has, after changing the hydrogen profile, four models that lie inside the errorbars. The transition region varies between 0.66M$_\odot$ and 0.83M$_\odot$, the initial convective core size is between 1.17M$_\odot$ and 1.24M$_\odot$, which implies ZAMS masses between 4.9M$_\odot$ and 5.1M$_\odot$. A point of concern is the fact that for all models the actual convective core mass is much smaller than the derived minimum core mass.
The 1.45M$_\odot$ models with an average mean molecular weight of $\bar{\mu} = 0.795$ and a core hydrogen abundance of $X_c = 0.1847, 0.2212$ and 0.2522 have also been recalculated with an adapted chemical profile. In brief, the initial ZAMS convec-

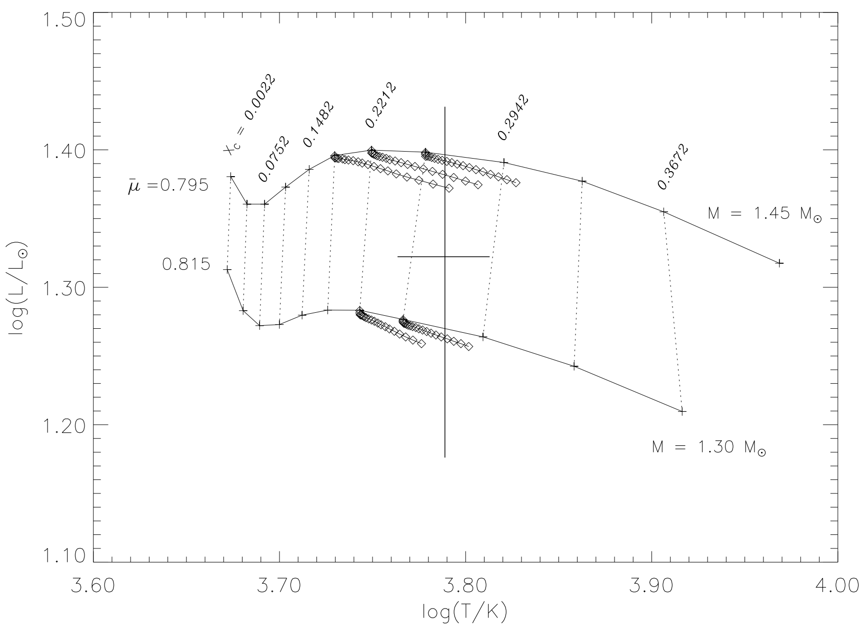

Figure 5.10: This figure shows five sequences (diamonts) of models with a changing slope in the chemical profile. All sequences start at a cross (discontinuous chemical profile) and move with decreasing slope to the right. The three sequences at the line of 1.45M$_\odot$ are calculated with an average mean molecular weight of $\bar{\mu} = 0.795$ and start respectively at central hydrogen abundances of $X_c = 0.1847, 0.2212$ and 0.2522. The two sequences at the line of 1.30M$_\odot$ are calcalated with an average mean molecular weight of $\bar{\mu} = 0.815$ and start respectively at central hydrogen abundances of $X_c = 0.2212$ and 0.2522. The point with errorbars is the observed point of Beer & Podsiadlowski (2002).

tive core masses could have been between 0.95M$_\odot$ and 1.38M$_\odot$, which implies total ZAMS masses between 4.2M$_\odot$ and 5.5M$_\odot$. Although the difference between the derived minimum core mass and the actual convective core mass is not as large as the difference for the 1.30M$_\odot$ models, all models, except the models with the flattest chemical profile, have a actual convective core that is smaller than the minimum derived core.

5.3.4 Summary

The secondary as observed by Beer & Podsiadlowski could be reproduced with stellar models that have a masses between 1.3 M$_\odot$ and 1.6 M$_\odot$, but not the entire mass range is investigated. Since the errorbars on the mass are large the average mean molecular weight could not be calculated very precise. If the

secondary has a mass of 1.30 $M_\odot$ the star is best reproduced by a model with a core hydrogen abundance of $X_c = 0.22$ and an average mean molecular weight of $\bar{\mu} = 0.815$. Zero-age main sequence stars with masses of $4.9 < M_i/M_\odot < 5.1$ could account, after significant mass loss for this star.
If the secondary has a mass of 1.45$M_\odot$ the star is best reproduced by a model with a core hydrogen abundance of $0.18 < X_c < 0.25$ and an average mean molecular weight of $\bar{\mu} = 0.795$. Zero-age main sequence stars with masses of $4.2 < M_i/M_\odot < 5.5$ could account, after significant mass loss for this star.

5.4 Conclusion

In this Chapter I have presented a new method for reconstructing the properties, i.e. mass, luminosity, temperature and radius, of an observed main sequence star. Using this method we are able to construct a stellar model of a certain mass that fullfils some constrains in luminosity, temperature and radius. This constructed stellar models gives also information about the hydrogen abundance in the core that has some relation with the age of the star, and also about the original mass of the convective core at Zero Age Main Sequence, which gives us the total initial mass that the progenitor of the current star should have had at ZAMS.
This method was applied to the secondary in the black hole binary system GRO J1655-40, because there is a huge discussion in literature about the masses of both components in this system.
The first star that is reconstructed using the method described in this chapter, was the secondary in GRO J1655-40 as observed by Orosz & Bailyn (1997). They claimed the secondary to have a mass $M_2 = 2.34 \pm 0.12 M_\odot$. Using this method we conclude that it is not likely for a star of 2.34$M_\odot$ to have the observed properties, but that a star with a mass between 2.20$M_\odot$ and 2.25$M_\odot$ would better fit to the observations. These models should be at the very end of core hydrogen burning ($X_c = 0.04$) and should have lost some mass during their evolution. Their initial ZAMS mass was calculated to be 2.8$M_\odot$.
The second reconstructed star is the secondary as investigated by Beer & Podsiadlowski (2002). They claimed the secondary to have a significantly lower mass of $1.45 \pm 0.35 M_\odot$. From the calculations in Section 5.3 we can conclude that the secondary can have a mass between 1.30$M_\odot$ and 1.45$M_\odot$, but perhaps also less massive and more massive, because not the whole parameter space in the mass and the average mean molecular weight is investigated. But using these two masses as the most likely, we derived the secondary to have a core hydrogen abundance of $X_c = 0.20 - 0.30$. The secondary should have lost a huge amount of mass during its evolution, because the Zero Age Main Sequence mass should have been between 4.1$M_\odot$ and 5.1$M_\odot$ for the 1.30$M_\odot$ star (between 2.8 and 3.8$M_\odot$ lost) and between 4.2$M_\odot$ and 5.5$M_\odot$ for the 1.45$M_\odot$ star (between 2.75 and 4.05$M_\odot$ lost).

The problem for almost all models, that the actual convective core mass is smaller than the computed minimum core mass, remains. A suggestion to solve this, is to construct a curved chemical profile. This should deliver a more realistic model, because the secondary mostly started mass transfer after spending a certain time on the main sequence, and not at the very beginning. After a period of evolution without mass loss the star starts a episode of evolution with mass loss, which causes the core too shrink more rapidly because of the two effects that work into the same direction, i.e. the shrinkage of the core due to the evolution and due to mass loss. These two effects give a flatter hydrogen profile from the start of mass loss, which could imply that the derived minimum core mass is lower.

From this method alone we can not conclude which mass of the secondary in GRO J1655-40 is the most likely. We need therefore additional information in the form of detailed binary evolutionary calculations and have to consider the orbital evolution as well. This will be done in the next chapter, where the resuls of chapter 3 and chapter 5 are combined into one general picture of the black hole binary system GRO J1655-40.

Chapter 6

Discussion

In this chapter we will compare the results from Chapter 3 and Chapter 5, to obtain some new insights in this system. In Chapter 3 we investigated detailed evolutionary calculations fot this system and tried to fit them to the observations. We concluded that Case B evolution is unlikely because of the high mass transfer rate that is incompatible with the transient behaviour the system displays. Therefore Case A evolutionary models were calculated in order to obtain a suitable solution for the evolution of this system that fits to the observations. For the observations we used the results obtained by Orosz & Bailyn (1997) and Beer & Podsiadlowksi (2002) who represent the most extreme values for the masses of the both stars in this system.
The results of Orosz & Bailyn were best represented with an evolutionary model that starts with an initial ZAMS model of $2.75 M_{\odot}$ that is now close to the end of core hydrogen burning. When we compare this result with the results obtained in Chapter 5 we can conclude that they are in remarkable agreement with each other. Using our artificially created stars we obtained as the best fit to the observations a star that has a present mass between 2.20 and $2.25 M_{\odot}$ and that had initially a ZAMS mass of $2.8 M_{\odot}$. This model has however an extreme low hydrogen abundance in the core.
The observationally derived results of Beer & Podsiadlowksi could not be reproduced with a detailed Case A evolutionary model, because of the thight constrains in the period and the luminosity. Using our artificially created stars we deduced an initial progenitor mass of the secondary between 4.1 and $5.5 M_{\odot}$. In this range we did not calculate detailed evolutionary models, because the system would have an initial unstable phase of mass transfer caused by the reversed mass ratio of the both components in the system. This unstable phase of mass transfer undoubtly would have caused non-conservative evolution, and the system would have lost probably a large amount of mass into the inter stellar environment. If this would have been the case, we would expect to see effects on the surrounding interstellar medium (cf. King & Kolb, 1999).

Figure 6.1 compares the chemical profile of a detailed evolutionary model

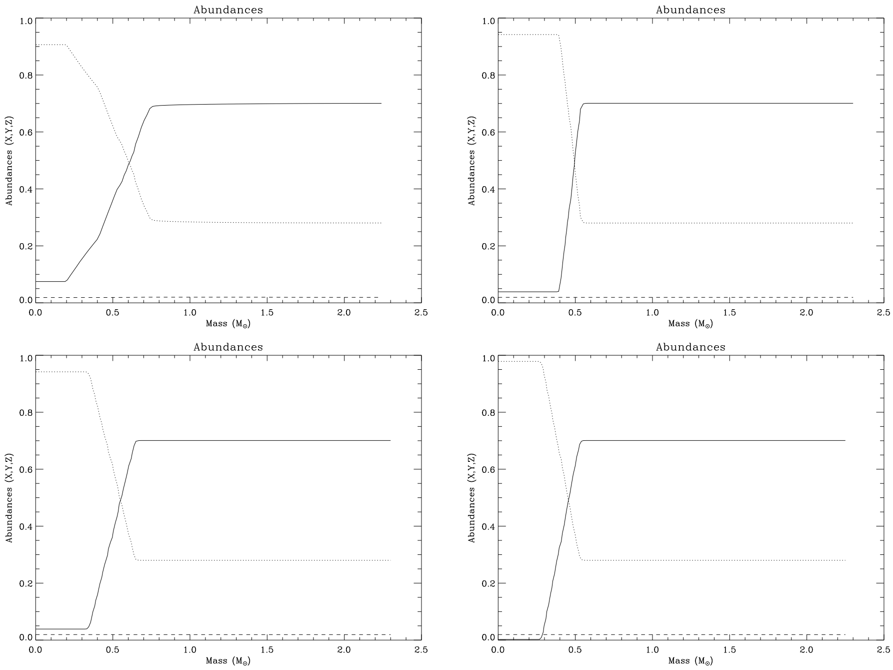

Figure 6.1: The upper-left panel is a profile from a detailed binary evolutionary model of which the evolutionary model in the Hertzsprung Russell Diagram is shown in Fig 3.5. The stellar model initially (ZAMS) had a mass of 3.5 $M_\odot$ and has an actual mass of 2.24 $M_\odot$, a temperature of $T_{\rm eff} = 6769K$, luminosity $L = 46.8L_\odot$ and a core hydrogen abundance of $X_{\rm c} = 0.07$.
The upper-right panel shows the abundance profile of a stellar model with a mass of 2.3 $M_\odot$, a luminosity of 46.8 $L_\odot$, temperature of 6634 K and a core hydrogen abundance of $X_{\rm c} = 0.04$.
The lower-left panel shows the abundance profile of a stellar model with a mass of 2.3 $M_\odot$, a luminosity of 50.1 $L_\odot$, temperature of 6570 K and a core hydrogen abundance of $X_{\rm c} = 0.04$.
The upper-right panel shows the abundance profile of a stellar model with a mass of 3.0 $M_\odot$, a luminosity of 41.7 $L_\odot$, temperature of 6665 K and a core hydrogen abundance of $X_{\rm c} = 0.002$.

of an initially 3.5 $M_\odot$ ZAMS star with the simplified chemical profiles of three stellar models. As can be seen, the luminosity, temperature and mass are all within the errorbars of the observed point of Orosz & Bailyn, but the hydrogen profile is in all three simplified models a bad approximation. The central hydrogen abundace is both in the detailed evolutionary model as in the simple numerical models very low, $0.002 < X_{\rm c} < 0.07$.

Chapter 7

Summary

This thesis is a report on the research I did on low mass black hole binary systems. I focussed my work on the low mass black hole binary GRO J1655-40, a well studied system which contains a black hole and a donor star that has Roche lobe overflow. Mostly the system is in quiescence, but sometimes it is very bright in X-rays. In the literature, the masses of both components and also the evolutionary status of the donor star, are still debated.

In order to understand in which evolutionary state the donor star is, we calculated several evolutionary models with different input parameters for the masses of both components and for the orbital period. We were able to reproduce one of the observations (by Orosz & Bailyn 1997) and concluded that the donor star still is a main sequence star, that should have evolved from an zero-age main sequence star with a mass 2.75 $M_\odot$ < M_i < 3.5 $M_\odot$. Another, very recent observation (by Beer & Podsiadlowski 2002), claims significantly lower masses for both components. We were not able to calculate an evolutionary model that goes through the errorbars of this observation.

One of the disadvantages of this approach is the trial-and-error nature. One needs lot of computertime in order to calculated appropriate models that fit the observations, since one is working in a large parameter space.

In order to avoid this trial-and-error approach, we developed a new method in which we can reconstruct step-by-step a stellar model that displays all the observed parameters. Important in this method is the calculation of a relation between the mass, the luminosity and the average mean molecular weight for main sequence star models. Using this relation we were able to construct stellar models in which we only had to make choices for the core mass and the gradient of the hydrogen profile.

With this method we were able to derive new constraints for the mass of the secondary in GRO J1655-40. The observed point by Orosz & Bailyn (1997) is best reproduced with a model with a mass between 2.20 $M_\odot$ and 2.30 $M_\odot$. This star initially had a mass between 2.8 $M_\odot$ and 3.5 $M_\odot$, what is in remarkable agreement with the detailed evolutionary calculations.

The observed point by Beer & Podsiadlowski (2002) is best reproduced by a stellar model with masses between 1.3 $M_\odot$ and 1.6 $M_\odot$. This star should initially have had a mass between 4.2 $M_\odot$ and 5.5 $M_\odot$, significantly higher as derived for the previous point. This implies that this star should have lost a huge amount of mass, $\gtrsim 3$ $M_\odot$, during the main sequence. Since there are no detailed binary evolutionary calculations, starting from these initial masses, we cannot check if it is possible to lose such an amount of mass during the main sequence. If this is possible, then the mass transfer rates would be quite high, causing the system to appear as a persistently bright system and not as a transient system, which is in disagreement with the observations. It therefore seems unlikely that stars with this high initial masses could evolve to stars that display the observed properties.

Conclusion of this research can be that the secondary in GRO J1655-40 is a main sequence star with a mass between 2.20 $M_\odot$ and 2.30 $M_\odot$ that initially had a mass between 2.8 $M_\odot$ and 3.5 $M_\odot$.

Bibliography

[1] Abramowicz M.A. & Kluźniak W., 2001, A&A, 374, L19

[2] Bailyn C.D., Orosz J.A., McClintock J.E. & Remillard R.A., 1995, Nature, 378, 157

[3] Bardeen J.M., 1970, Nature, 226, 64

[4] Beer M. & Podsiadlowski Ph., 2002, MNRAS, 331, 351

[5] Brandt W.N., Podsiadlowski Ph. & Sigurdsson S., 1995, MNRAS, 277, L35

[6] Braun H., 1997, Ph.D. Thesis, LMU München

[7] Braun H. & Langer N., 1995, A&A, 297, 483

[8] Brown G.E., Lee C.-H. & Tauris T.M., 2001, NewA, 6, 331B

[9] Brown G.E., Lee C.-H. , Wijers R.A.M.J., Lee H.K., Israelian G. & Bethe H.A., 2000, NewA, 5, 191

[10] Caroll B.W. & Ostlie D.A., 1996, *An Introduction to Modern Astrophysics*, Addison-Wesley Publishing Company, Inc., Reading, Massachusetts

[11] Cui W., Zhang S.N., Chen W., 1998, ApJ, 492, L53

[12] Eggleton P.P., 1983, ApJ, 268, 368

[13] Esin A.A., Lasota J.P. & Hynes R.I., 2000, A&A, 354, 987

[14] Hjellming R.M. & Rupen M.P., 1995, Nature, 375, 464

[15] van der Hooft F., Groot P.J. Shahbaz T., Augusteijn T., Casares J., Dieters S., Greenhill J., Hill K., Scheers L.H.A., Naber R.M., de Jong J.A., Charles P.A. & van Paradijs J., 1997, MNRAS, 286, L43

[16] van der Hooft F., Heemskerk M.H.M., Alberts F. & van Paradijs J., 1998, A&A, 329, 538

[17] Hurley J.R., Pols O.R., Tout C.A., 2000, MNRAS, 315, 543

[18] Iglesias C.A. & Rogers F.J., 1996, ApJ, 464, 943

[19] Israelian G., Rebolo R., Basri G., Casares J. & Martin E.L., 1999, Nature, 401, 142

[20] King A.R., Frank J., Kolb U. & Ritter H., 1997, ApJ, 484, 884

[21] King A.R. & Kolb U., 1999, MNRAS, 305, 654

[22] King A.R., Kolb U. & Burderi L., 1996, ApJ, 464, L127

[23] King A.R., Kolb U. & Szuszkiewicz, 1997, ApJ, 488, 89

[24] King A.R., Schenker K., Kolb U. & Davies M.B., 2001, MNRAS, 321, 327.

[25] Kolb U., King A.R., Ritter H. & Frank J., 1997, ApJ, 485, L33

[26] Kolb U., 1998, MNRAS, 297, 419

[27] Kippenhahn R. & Weigert A., 1990, *Stellar structure and evolution*, Springer, Berlin

[28] Langer N., 1991, A&A, 252, 669

[29] Langer N., 1998, A&A, 329, 551

[30] Lee C.H., Brown G.E. & Wijers R.A.M.J., 2001, astro-ph/0109538

[31] McHardy I.M., Lawrence A., Pye J.P., Pounds K.A., 1981, MNRAS, 197,893

[32] Meier D.L., 2001, ApJ, 548, L9

[33] Nelemans G., Tauris T.M. & van den Heuvel E.P.J., 1999, A&A, 352, L87

[34] Orosz J.A. & Bailyn C.D. 1997, ApJ, 477, 876

[35] Osaki Y., 1996, PASP, 108, 39

[36] Paradijs J. van, 1996, ApJ, 464, L139

[37] Podsiadlowski Ph., 2002, private communication

[38] Popper D.M., 1980, Ann. Rev. Astron. Astrophys, 18, 115

[39] Press W.H., Teukolsky S.A., Vetterling W.T. & Flannery B.P., 1992, *Numerical Recipes in Fortran*, Cambridge University Press, Cambridge

[40] Regős E., Tout C.A. & Wickramasinghe D., 1998, ApJ, 509, 362

[41] Ritter H., 1988, a&A, 202, 93

[42] Ritter H., 1996, in Wijers R.A.M.J., Davies M.B., Tout C.A., eds, NATO ASI Series C, Vol. 477, Evolutionary Processes in Binary Stars. Kluwer, Dordrecht, p. 233

[43] Rosat Website, ROSAT Wrap-Up, September 2002
http://heasarc.gsfc.nasa.gov/docs/rosat/taps.html

[44] Shahbaz T., van der Hooft F., Casares J. Charles P.A. & van Paradijs J., 1999, MNRAS, 306, 89

[45] Shahbaz T., Groot P., Phillips S.N., Casares J., Charles P.A. & van Paradijs J., 2000, MNRAS, 314, 747

[46] Shapiro S.L. & Teukolsky S.A., 1983, *Black Holes, White Dwarfs and Neutron Stars*, Wiley-Interscience

[47] Smak J., 1983, ApJ, 272, 234

[48] Verbunt F., 2000, Lecture Notes, SIU, Utrecht

[49] Verbunt F., 2001, in Kaper L., Heuvel E.P.J. van den & Woudt P.A., eds, Proceedings of the ESO Workshop held at Garching, Germany, 6-8 September 1999. Springer, p. 279

[50] Wellstein S. & Langer N., 1999, A&A, 350, 148

[51] Wijers R.A.M.J., 1996, in Wijers R.A.M.J., Davies M.B., Tout C.A., eds, NATO ASI Series C, Vol. 477, Evolutionary Processes in Binary Stars. Kluwer, Dordrecht, p. 327

[52] Zhang S.N., Wilson C.A., Harmon B.A., Fishman G.J., Wilson R.B., Paciesas W.S., Scott M. & Rubin B.C., 1994, IAU Circ. 6046

[53] Zhang S.N., Cui W., Chen W., 1997, ApJ, 482, L155

Acknowlegdements

At first I would like to thank Norbert Langer, my supervisor, for all the help he gives me during the time I was working on my research. In the first months you critically followed my work, but after a while you grew enthousiastic, which motivated me to carry on. Thanks for all the enlightning discussions!
Onno, although you were not officially connected to my research, I could always ask you for help. Also thanks to the other members of the research group, especially Yoon for help with the code.
Also thanks to Phillip Podsiadlowski for taking time to compare his results with mine and making helpful comments.
I thank Cees Bassa, Gemma Janssen and Joke Meijer for working one year in the same office and for the convivial atmosphere. Gemma thanks for the litres of thea you made.
At last I want to thank my parents wo were always interested in what I was doing, but scarcely did understand what I was doing.